

Collective Mode at Lifshitz Transition in Iron-Pnictide Superconductors

Jose P. Rodriguez¹

¹*Department of Physics and Astronomy,
California State University at Los Angeles, Los Angeles, California 90032.*

Abstract

We obtain the exact low-energy spectrum of two mobile holes in a t - J model for an isolated layer in an iron-pnictide superconductor. The minimum d_{xz} and d_{yz} orbitals per iron atom are included, with no hybridization between the two. After tuning the Hund coupling to a putative quantum critical point (QCP) that separates a commensurate spin-density wave from a hidden-order antiferromagnet at half filling, we find an s -wave hole-pair groundstate and a d -wave hole-pair excited state. Near the QCP, both alternate in sign between hole Fermi surface pockets at the Brillouin zone center and emergent electron Fermi surface pockets at momenta that correspond to commensurate spin-density waves (cSDW). The dependence of the energy splitting with increasing Hund coupling yields evidence for a true QCP in the thermodynamic limit near the putative one, at which the s -wave and d -wave Cooper pairs are degenerate. A collective s -to- d -wave oscillation of the macroscopic superconductor that couples to orthorhombic shear strain is also identified. Its resonant frequency is predicted to collapse to zero at the QCP in the limit of low hole concentration. This implies degeneracy of Cooper pairs with s , d and $s + id$ symmetry in the corresponding quantum critical state. We argue that the critical state describes Cooper pairs in hole-doped iron superconductors at the Lifshitz transition, where electron bands first rise above the Fermi level. We thereby predict that the s -to- d -wave collective mode observed by Raman spectroscopy in $\text{Ba}_{1-x}\text{K}_x\text{Fe}_2\text{As}_2$ at optimal doping should also be observed at higher doping near the Lifshitz transition.

I. INTRODUCTION

The symmetry of the Cooper pairs of electrons in iron-pnictide high-temperature superconductors remains a subject of controversy. A stack of weakly coupled square lattices of iron atoms is the common structural feature in these materials. Early calculations of the electronic band structure within the density functional approximation predicted nested two-dimensional (2D) Fermi surfaces^{1,2}, with hole pockets centered at zero 2D momentum, and with electron pockets centered at 2D momenta $\hbar(\pi/a)\hat{x}$ and $\hbar(\pi/a)\hat{y}$. Here a is the intralayer Fe-Fe separation. The predicted Fermi surfaces were later confirmed experimentally by angle-resolved photo-emission spectroscopy (ARPES)^{3,4}. Early calculations based on the above nested electronic structure also predicted an S^{+-} symmetry for the wavefunction of the Cooper pair that alternates in sign between the hole pockets and the electron pockets because of spin-fluctuation exchange at the nesting vectors^{5,6}. Nearly degenerate Cooper pairs with d -wave symmetry are also predicted to exist because of such spin-fluctuation exchange^{7,8}, however.

The discovery of the hole-doped series $\text{Ba}_{1-x}\text{K}_x\text{Fe}_2\text{As}_2$ poses a challenge to the proposal of S^{+-} Cooper pair symmetry in iron-pnictide superconductors⁹. High-temperature superconductivity exists in a considerable range about optimal doping¹⁰ at $x \cong 0.4$, where $T_c \cong 38$ K. ARPES in this range of doping finds evidence for an s -wave gap both on hole Fermi surfaces at zero 2D momentum and on small electron Fermi surfaces at commensurate spin-density wave (cSDW) momenta^{4,11}. The low-temperature dependence of the London penetration depth and of the thermal conductivity at optimal doping^{12,13} are consistent with such s -wave superconducting gaps. ARPES also finds that the small electron Fermi surface pockets that exist at optimal doping are *absent* in the end-member compound¹⁴ at $x = 1$, however, where $T_c = 3$ K. Specifically, ARPES and thermo-electric measurements find evidence for a continuous Lifshitz transition at a concentration inside the range $0.5 < x < 1$, where the electron bands at cSDW momenta first rise above the Fermi level^{15,16}. A recent calculation based on density-functional theory (DFT) argues that the Lifshitz transition is a result of the (Ba,K) alloy¹⁷. At optimal doping, however, ARPES finds strong mass renormalizations of the electron bands at cSDW momenta by up to a factor of six compared to DFT¹⁴. This failure suggests that strong on-site Coulomb repulsion should be taken into account¹⁸⁻²¹.

We reveal the nature of a single Cooper pair in a local-moment t - J model for hole-doped iron superconductors characterized by large on-site Coulomb repulsion. Two mobile holes roam over a 4×4 periodic lattice of spin-1 iron atoms that contain only d_{xz} and d_{yz} orbitals. They coincide with the orbital character of the most intense bands seen by ARPES at the Brillouin zone center and at cSDW momenta in optimally doped¹⁵ $\text{Ba}_{1-x}\text{K}_x\text{Fe}_2\text{As}_2$. The hole bands centered at zero 2D momentum are fixed by the band structure (t), while the electron bands are emergent at nesting wave vectors because of proximity to a cSDW state that is favored by antiferromagnetic frustration (J)^{18,19}. In the case of one mobile hole, both bands cross the Fermi level at a critical Hund coupling that is of moderate strength²². A comparison with the results of Schwinger-boson-slave-fermion meanfield theory suggests that the latter coincides with a quantum critical point (QCP) that separates a cSDW at strong Hund coupling from a hidden-order magnet at weak Hund coupling²². Unlike previous exact numerical studies of pairing in two-orbital 2D superconductors with on-site Coulomb repulsion²³, we thereby avoid accounting for the electron pockets with fine-tuned hopping matrix elements²⁴ that result in an unphysical hole Fermi surface pocket⁸. The theory necessarily predicts a Mott insulator state at half filling. Recent experimental evidence for an insulator-superconductor transition in single-layer FeSe supports this prediction^{25,26}. It is related to the present hole-doped study by the application of an exact particle-hole transformation²⁷.

After tuning the Hund coupling to the QCP, and in the absence of hybridization between the d_{xz} and d_{yz} orbitals, we find that the groundstate is a spin-0 Cooper pair with primarily S^{+-} symmetry. It is in a bonding superposition of orbitally ordered $d_{yz}^{2(+)}$ and $d_{xz}^{2(-)}$ singlet pairs that alternate in sign between respective hole and electron pockets. (Cf. ref.²⁸.) The S^{+-} hole pair is well separated from a continuum of states, but close by in energy to an antibonding D^{+-} Cooper pair. (See Fig. 1d, blue versus red.) The macroscopic superconductor will exhibit an internal Josephson effect between the two species of orbitally ordered Cooper pairs²⁹⁻³². We thereby predict a neutral spin-0 collective mode in the macroscopic superconducting state that exhibits orbital pair oscillations. It couples directly to orthorhombic shear^{33,34}.

Last, the exact energy difference separating the D^{+-} and the S^{+-} hole-pair states tends to zero linearly with increasing Hund coupling near the QCP. (See Fig. 5b.) By comparison with mean-field theory and exact results for one mobile hole²², we argue in the Discussion

section that the quantum critical state³⁵, where S^{+-} and D^{+-} Cooper pairs become degenerate, coincides with the Lifshitz transition, where electron bands at cSDW momenta first rise above the Fermi level^{10,15,16}. This picture implies remnant Cooper pairs of opposite sign on the emergent electron bands that lie above the Fermi level at subcritical Hund coupling. (See Figs. 2b and 6.) A recent analysis of a phenomenological model for overdoped $\text{Ba}_{1-x}\text{K}_x\text{Fe}_2\text{As}_2$ reaches a similar conclusion³⁶. The present theory also then predicts that the in-gap s -to- d -wave collective mode observed recently by Raman spectroscopy in optimally doped $\text{Ba}_{1-x}\text{K}_x\text{Fe}_2\text{As}_2$ will also be observed at the Lifshitz transition at higher doping^{37,38}.

II. LOCAL-MOMENT MODEL

The Hamiltonian for the two-orbital t - J model on a square lattice of iron atoms reads^{21,22}

$$\begin{aligned}
H = & \sum_{\langle i,j \rangle} \left[-(t_1^{\alpha,\beta} \tilde{c}_{i,\alpha,s}^\dagger \tilde{c}_{j,\beta,s} + \text{h.c.}) + J_1^{\alpha,\beta} (\mathbf{S}_{i,\alpha} \cdot \mathbf{S}_{j,\beta} + \frac{1}{4} n_{i,\alpha} n_{j,\beta}) \right] + \\
& \sum_{\langle\langle i,j \rangle\rangle} J_2^{\alpha,\beta} (\mathbf{S}_{i,\alpha} \cdot \mathbf{S}_{j,\beta} + \frac{1}{4} n_{i,\alpha} n_{j,\beta}) + \sum_i (J_0 \mathbf{S}_{i,d-} \cdot \mathbf{S}_{i,d+} + U'_0 \bar{n}_{i,d+} \bar{n}_{i,d-}).
\end{aligned} \tag{1}$$

Above, $\tilde{c}_{i,\alpha,s} = b_{i,\alpha,s} f_{i,\alpha}^\dagger$ is the destruction operator for an electron of spin s , at site i , in orbital α . Also, $\mathbf{S}_{i,\alpha} = \frac{1}{2} \sum_{s,s'} \tilde{c}_{i,\alpha,s}^\dagger \boldsymbol{\sigma}_{s,s'} \tilde{c}_{i,\alpha,s'}$ is the spin operator in units of \hbar , $n_{i,\alpha} = \sum_s \tilde{c}_{i,\alpha,s}^\dagger \tilde{c}_{i,\alpha,s}$ measures the net occupation per site-orbital, while $\bar{n}_{i,\alpha} = 1 - n_{i,\alpha}$ counts holes instead. Electrons live on the $d+ = d_{(x+iy)z}$ and/or the $d- = d_{(x-iy)z}$ orbitals. Repeated orbital and spin indices in the hopping and Heisenberg exchange terms above are summed over. These terms in the Hamiltonian (1) are in turn summed over nearest neighbor and next-nearest neighbor links, $\langle i, j \rangle$ and $\langle\langle i, j \rangle\rangle$. Double occupancy at a site-orbital is projected out by enforcing the constraint

$$1 = b_{i,\alpha,\uparrow}^\dagger b_{i,\alpha,\uparrow} + b_{i,\alpha,\downarrow}^\dagger b_{i,\alpha,\downarrow} + f_{i,\alpha}^\dagger f_{i,\alpha}, \tag{2}$$

where $b_{i,\alpha,\uparrow}$ and $b_{i,\alpha,\downarrow}$ are the destruction operators for a pair of Schwinger bosons, and where $f_{i,\alpha}$ is the destruction operator for a spinless slave fermion^{39,40}. In order to reduce finite-size effects, we have added a *repulsive* interaction to the Heisenberg exchange terms above. The net interaction between nearest neighbors ($n = 1$) and between next-nearest neighbors

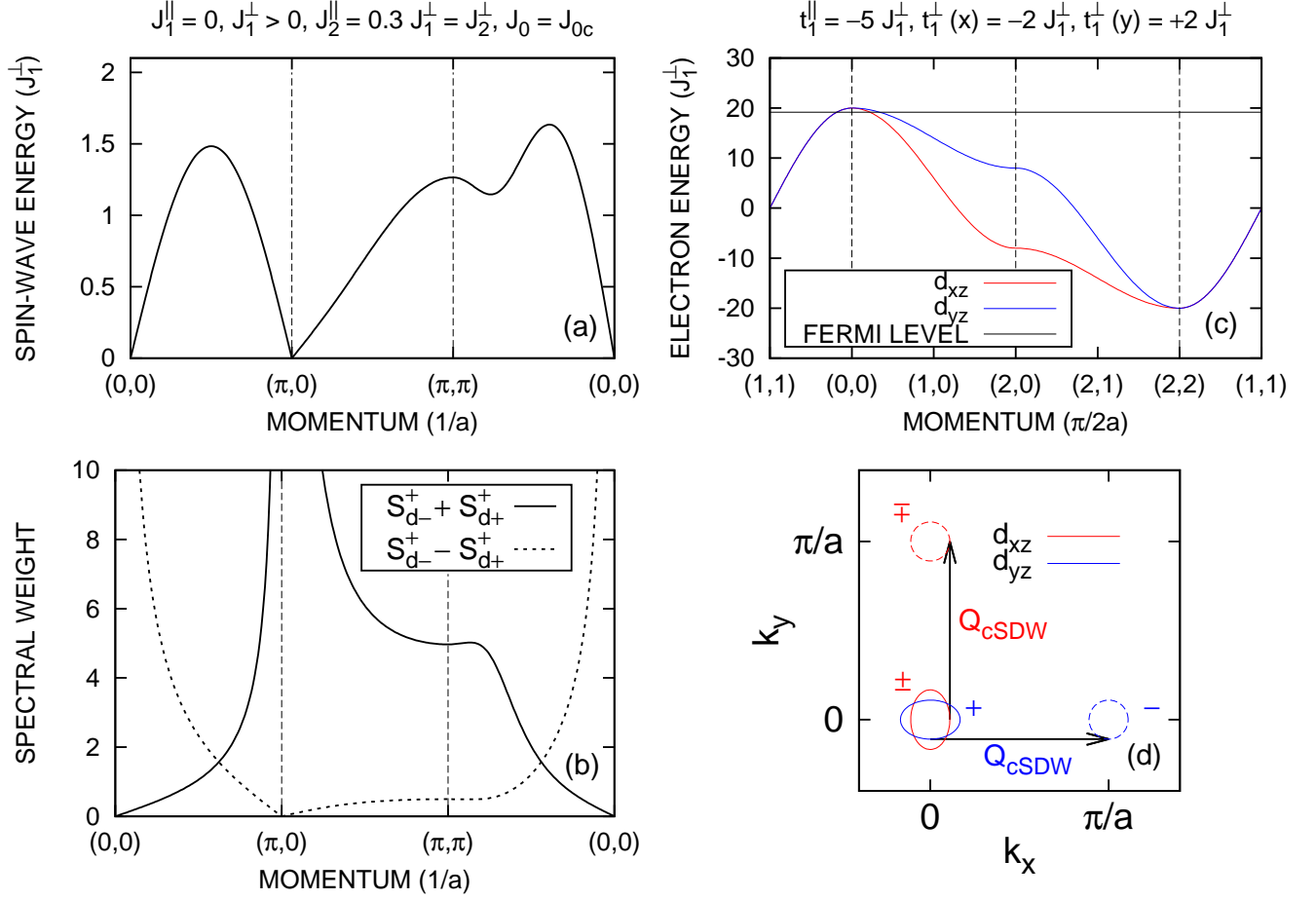


FIG. 1: The critical low-energy spectrum (a)-(b) of the two-orbital Heisenberg model that corresponds to Eq. (1) in the linear spin-wave approximation (ref.²⁰). The Hund coupling is set to $-J_{0c} = 0.8 J_1^\perp$. True ($q_0 = 0$) and hidden ($q_0 = \pi$) spinwaves are degenerate. Shown also is (c) the band structure and (d) emergent nesting (ref.²²) for the two-orbital t - J model, Eq. (1). The Fermi-level in panel (c) corresponds to a non-optimal half metal phase obtained from Schwinger-boson-slave-fermion meanfield theory at subcritical Hund coupling (ref.²²).

($n = 2$) is thereby pure spin exchange: $\frac{1}{2} J_n^{\alpha, \beta} P_{i, \alpha; j, \beta}$. Here, the operator $P_{i, \alpha; j, \beta}$ exchanges spins on site-orbitals (i, α) and (j, β). Observe the invariance of the Hamiltonian under the following internal global gauge transformation: $\tilde{c}_{i, d\pm, s} \rightarrow e^{\pm i\delta_0} \tilde{c}_{i, d\pm, s}$ and $t_1^{d\pm d\mp} \rightarrow e^{\pm 2i\delta_0} t_1^{d\pm d\mp}$. It is equivalent to a rotation of the orbital coordinates (x, y) by an angle δ_0 . The t - J model (1) is then invariant under an arbitrary rotation of the two orbitals about the z axis.

Below, we will provide evidence that the two-orbital t - J model is unstable to the formation of local intra-orbital Cooper pairs in the vicinity of a QCP that separates cSDW order from hidden magnetic order. The second column in Table I coincides with the parameter range of

filling, bands	$J_1^{\parallel} < J_1^{\perp}$	$J_1^{\parallel} > J_1^{\perp}$
half filling, none	hidden ferromagnet: $(\pi, 0, 0)$	hidden Néel: $(\pi, \pi/a, \pi/a)$
hole dope, hole bands at Γ	hidden half metal, FS pockets at Γ	nested cSDW metal?

TABLE I: Groundstate of two-orbital t - J model (1). Hund coupling is tuned to the QCP at half filling, which separates a cSDW at strong Hund coupling from hidden magnetic order at weak Hund coupling (ref.²⁰). The 3-vector (π, k_x, k_y) describes the hidden magnetic order.

the model. We will further show that an internal Josephson effect exists, specifically, between d_{yz} - d_{yz} and d_{xz} - d_{xz} singlet Cooper pairs. Before doing so, however, we first demonstrate how emergent electron bands begin to nest with hole Fermi surface pockets at the QCP.

III. COHERENT HOLE BANDS AND EMERGENT ELECTRON BANDS

Semi-classical calculations of the Heisenberg model that corresponds to (1) at half filling find a QCP that separates a cSDW at strong Hund coupling from a hidden antiferromagnet at weak Hund coupling if off-diagonal frustration is present²⁰: e.g. $J_1^{\parallel} = 0$, $J_1^{\perp} > 0$, and $J_2^{\parallel} = J_2^{\perp} > 0$. The antiferromagnetic sublattices of the hidden-order state are the $d+$ and $d-$ orbitals. In particular, the groundstate at large electron spin s_0 is the spin texture $\nearrow_{d-} \searrow_{d+}$. Ideal hopping of holes within an antiferromagnetic sublattice, $t_1^{\parallel} < 0$ and $t_1^{\perp} = 0$, leaves such hidden magnetic order intact. In such case, a mean-field treatment of (1) and (2) at Hund coupling below the QCP reveals a half metal with doubly-degenerate Fermi surface pockets at zero 2D momentum that are circular and hole-type^{21,22}. The second column in Table I summarizes the above. Below, we demonstrate that emergent electron bands at cSDW momenta are also predicted within the mean-field approximation.

Electronic structure is revealed by the propagator for one electron at energy ω , at 3-momentum $k = (k_0, \mathbf{k})$. Here the quantum numbers $k_0 = 0$ and π represent bonding and anti-bonding superpositions of the $d-$ and $d+$ orbitals, which are respectively the d_{xz} and the $(-i)d_{yz}$ orbitals. The latter are good quantum numbers in the absence of hybridization, which is the case throughout. Within a mean-field approximation for the half-metal state, where the constraint against double occupancy (2) is enforced on average over the bulk, the

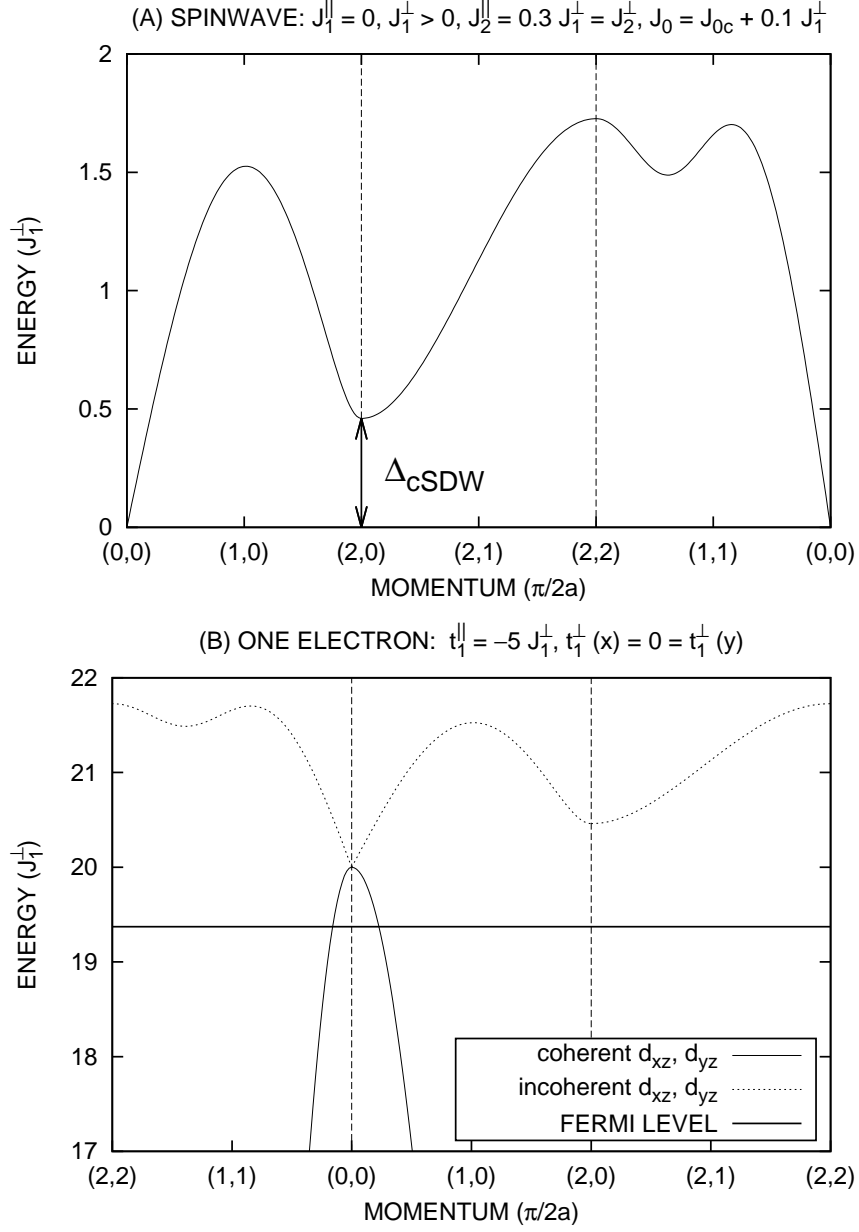


FIG. 2: (a) The energy-dispersion relation for spinwaves (Schwinger bosons) in the half-metal state near the QCP and (b) the corresponding imaginary part of the one-electron propagator near half filling, Eq. 4, at site-orbital concentration $x = 0.01$. Intrinsic broadening due to incoherent contributions in Eq. 3 is not shown. (See text.)

one-electron propagator is given by the expression²¹

$$G(k, \omega) = \frac{1}{\mathcal{N}} \sum_q \left[(\cosh \theta_{q+k})^2 \frac{n_B[\omega_b(q+k)] + n_F[\varepsilon_f(q)]}{\omega - \omega_b(q+k) + \varepsilon_f(q)} + (\sinh \theta_{q+k})^2 \frac{n_B[\omega_b(q+k)] + n_F[-\varepsilon_f(q)]}{\omega + \omega_b(q+k) + \varepsilon_f(q)} \right]. \quad (3)$$

Above, $\omega_b = (\Omega_{\parallel}^2 - \Omega_{\perp}^2)^{1/2}$ is the energy dispersion of the spin-carrying Schwinger bosons, while $\varepsilon_f(\mathbf{k}) = 8s_0t_1^{\parallel}\gamma_1(\mathbf{k}) - \mu$ is the energy dispersion of the charge-carrying slave fermions measured with respect to the chemical potential μ . Both are degenerate in the orbital channels $k_0 = 0$ and π . Here²¹,

$$\begin{aligned} \Omega_{\parallel}(k) &= s_0 \sum_{n=0,1,2} z_n J_n^{\prime\perp} - 4 \sum_{n=1,2} (s_0 J_n^{\parallel} + t_n^{\parallel} x) [1 - \gamma_n(\mathbf{k})], \\ \Omega_{\perp}(k) &= s_0 e^{ik_0} \sum_{n=0,1,2} z_n J_n^{\prime\perp} \gamma_n(\mathbf{k}), \end{aligned}$$

and $\gamma_1(\mathbf{k}) = \frac{1}{2}(\cos k_x a + \cos k_y a)$. Above, $\gamma_0(\mathbf{k}) = 1$ and $\gamma_2(\mathbf{k}) = \frac{1}{2}(\cos k_+ a + \cos k_- a)$, with $k_{\pm} = k_x \pm k_y$, while $z_0 = 1$ and $z_1 = 4 = z_2$ are coordination numbers, and while $J' = (1-x)^2 J$. Also above, n_B and n_F denote the Bose-Einstein and the Fermi-Dirac distributions, while $\mathcal{N} = 2N_{\text{Fe}}$ denotes the number of site-orbitals on the square lattice of N_{Fe} iron atoms. Last, the coherence factors for Schwinger bosons that appear in (3) are set by $\cosh 2\theta = \Omega_{\parallel}/\omega_b$ and $\sinh 2\theta = \Omega_{\perp}/\omega_b$. Ideal Bose-Einstein condensation (BEC) of the Schwinger bosons in the Goldstone mode shown in Fig. 2a results in the following coherent contribution to the electronic spectral function²¹ at zero temperature and at large electron spin s_0 : $\text{Im} G_{\text{coh}}(k, \omega) = s_0 \pi \delta[\omega + \varepsilon_f(k)]$. It reveals degenerate hole bands for d_{xz} and d_{yz} orbitals centered at zero 2D momentum, with circular Fermi surfaces of radius $k_F a = (4\pi x)^{1/2}$. Here, x denotes the concentration of holes per iron site, per orbital. The hole Fermi surface pockets at $\omega = 0$ are depicted by Fig. 1d. Mass anisotropy has been added to distinguish between the two orbitals. At energies above the Fermi level, $\omega > 0$, the remaining contribution from incoherent excitations $\text{Im} G_{\text{inc}}(k, \omega)$ are exclusively due to the first fermion term in (3). It is easily evaluated in the limit near half-filling, $k_F a \rightarrow 0$, at large t/J :

$$\text{Im} G_{\text{inc}}(k, \omega) \cong \pi x \left(\frac{1}{2} + \frac{1}{2} \frac{\Omega_{\parallel}}{\omega_b} \Big|_{\mathbf{k}} \right) \delta[\omega - \epsilon_F - \omega_b(\mathbf{k})]. \quad (4)$$

Figure 2b displays the emergent electron bands predicted above. They lie $\epsilon_F + \Delta_{\text{cSDW}}$ above the Fermi level, with degenerate minima at both cSDW wavenumbers $(\pi/a)\hat{\mathbf{x}}$ and

$(\pi/a)\hat{\mathbf{y}}$, for both the d_{xz} and d_{yz} orbitals. Here, $\epsilon_F = (2s_0)|t_1^\parallel|(k_F a)^2$ is the Fermi energy, and Δ_{cSDW} is the spin gap at cSDW wavenumbers shown by Fig. 2a. It vanishes at the QCP as $\Delta_{cSDW} \propto \text{Re}(J_0 - J_{0c})^{1/2}$, with a critical Hund coupling²¹

$$-J_{0c} = 2(J_1^\perp - J_1^\parallel) - 4J_2^\parallel - (1-x)^{-2}s_0^{-1}2t_1^\parallel x. \quad (5)$$

The emergent bands exhibit intrinsic broadening in frequency, which can be calculated outside the critical region, at large t/J : $\Delta\omega \sim k_F |\nabla\omega_b|_{\mathbf{k}}$. It remains small at the previous minima. Notice the divergence of the spectral weight in (4) at cSDW wavenumbers, as the cSDW spin gap vanishes at the QCP. It yields the bound $\Delta_{cSDW} > k_F v_0$ that guarantees the validity of (4). Here, v_0 denotes the velocity of cSDW spinwaves at the QCP. (See ref.²¹ and Appendix A.) The same criterion results in the bound $|\mathbf{k}| > k_F$, which guarantees the validity of (4) near $\mathbf{k} = 0$. Last, Fig. 2 displays how the emergent electron bands predicted by (4) inherit the mass anisotropy of the spinwaves at cSDW momenta.

At one electron less than half filling, exact calculations of the two-orbital t - J model (1) over a 4×4 lattice of iron atoms obtain a low-energy spectrum that compares well with the emergent electron bands (4) shown by Fig. 2b, but in the absence of Hund's rule. (See ref.²¹, Fig. 3a.) Adding inter-orbital electron hopping, $t_1^\perp(\hat{\mathbf{x}}) < 0$, with $t_1^\perp(\hat{\mathbf{y}}) = -t_1^\perp(\hat{\mathbf{x}})$, breaks orbital degeneracy both in the coherent hole bands and in the emergent electron bands. Exact results over a 4×4 lattice of iron atoms find that such inter-orbital hopping results in an energy splitting between the d_{xz} and d_{yz} hole states at momenta $\pm(\pi/2a)\hat{\mathbf{x}}$ and $\pm(\pi/2a)\hat{\mathbf{y}}$ that reflects the mass anisotropies depicted by Fig. 1d. (See ref.²², Figs. 4 and 5.) The exact results also find emergent electron bands at cSDW wave numbers $\mathbf{Q}_0 = (\pi/a)\hat{\mathbf{y}}$ and $\mathbf{Q}_\pi = (\pi/a)\hat{\mathbf{x}}$ with respective d_{xz} and d_{yz} orbital character²². They become degenerate with the doubly-degenerate groundstates at zero 2D momentum at the QCP, where Hund coupling is tuned to the critical value $-J_{0c} = 1.733 J_1^\perp$. Heisenberg-exchange and electron-hopping parameters coincide with those set in Fig. 1. Last, the first-excited states for the specific orbital k_0 at neighboring momenta $\mathbf{Q}_{k_0} \pm (\pi/2a)\hat{\mathbf{x}}$ and $\mathbf{Q}_{k_0} \pm (\pi/2a)\hat{\mathbf{y}}$ are nearly degenerate in such case. (See ref.²², Fig. 5.) This is consistent with emergent electron bands at cSDW momenta with nearly isotropic effective masses near the QCP.

IV. LOW-ENERGY SPECTRUM OF HOLE PAIR

The exact low-energy spectrum of a pair of holes that roam over a periodic 4×4 square lattice of iron atoms governed by the two-orbital t - J model (1) can be obtained numerically. The total spin along the z axis is constrained to $\sum S_z = 0$. Quantum states are defined by a given spin background over the entire lattice combined with a pair of spin-up and spin-down site-orbitals designated as holes. The former defines the ensemble of Schwinger bosons, which we treat in occupation space, while the latter defines the pair of slave fermions, which we treat in first quantization. Translation symmetry and a combination of spin-flip symmetry with slave-fermion exchange is also included, as well as reflection symmetries that leave momenta invariant. Due to the absence of hybridization among the d_{xz} and d_{yz} holes, orbital swap symmetry $P_{d,\bar{d}}$ is further added to the list: $d+ \leftrightarrow d-$. For example, including an even parity reflection about the x axis, an even parity spin-flip, plus even parity orbital swap reduces the dimension of the Hilbert space with net momentum $\hbar(\pi/2a)\hat{x}$ to 601 878 172 states. The ARPACK subroutine library is exploited to obtain low-energy eigenstates via the Lanczos technique⁴¹. Also, matrix-vector products are accelerated throughout by running parallel OpenMP threads.

Half Filling. In the absence of mobile holes, the two-orbital t - J model (1) describes a frustrated antiferromagnetic insulator. Figure 3 shows the exact critical spectrum of the corresponding two-orbital Heisenberg model over a 4×4 lattice of iron atoms, with exchange coupling constants $J_1^\parallel = 0$, $J_1^\perp > 0$, and $J_2^\parallel = 0.3 J_1^\perp = J_2^\perp$. The Hund coupling is tuned to a critical value of $-J_{0c} = 1.35 J_1^\perp$, at which point true spinwaves at cSDW momenta that have even parity under swap of the $d+$ and $d-$ orbitals become degenerate with hidden-order spinwaves at zero 2D momentum that have odd parity under such orbital swap. The hidden-order spinwave (hSW) signals long-range antiferromagnetic correlations across the $d+$ and $d-$ orbitals at wavenumber $\mathbf{Q} = 0^{20}$, $\nearrow_{d-} \searrow_{d+}$, with order parameter

$$\langle S_{d-}^+(\mathbf{Q}) - S_{d+}^+(\mathbf{Q}) \rangle = i\hbar \sum_{\mathbf{k}} \langle \tilde{c}_{d_{xz},\uparrow}^\dagger(\mathbf{k}) \tilde{c}_{d_{yz},\downarrow}(\mathbf{k} + \mathbf{Q}) - \tilde{c}_{d_{yz},\uparrow}^\dagger(\mathbf{k}) \tilde{c}_{d_{xz},\downarrow}(\mathbf{k} + \mathbf{Q}) \rangle. \quad (6)$$

Here, $\tilde{c}_{o,s}(\mathbf{k})$ destroys a strongly correlated electron of spin s in orbital o that carries momentum $\hbar\mathbf{k}$. The hidden magnetic order parameter (6) is an orbital singlet, which is odd (“red”) under $P_{d,\bar{d}}$, and it manifestly probes *inter-orbital nesting*²². Such hidden magnetic order becomes possible at weak intra-orbital Heisenberg exchange, $J_1^\parallel < J_1^\perp$, at subcritical

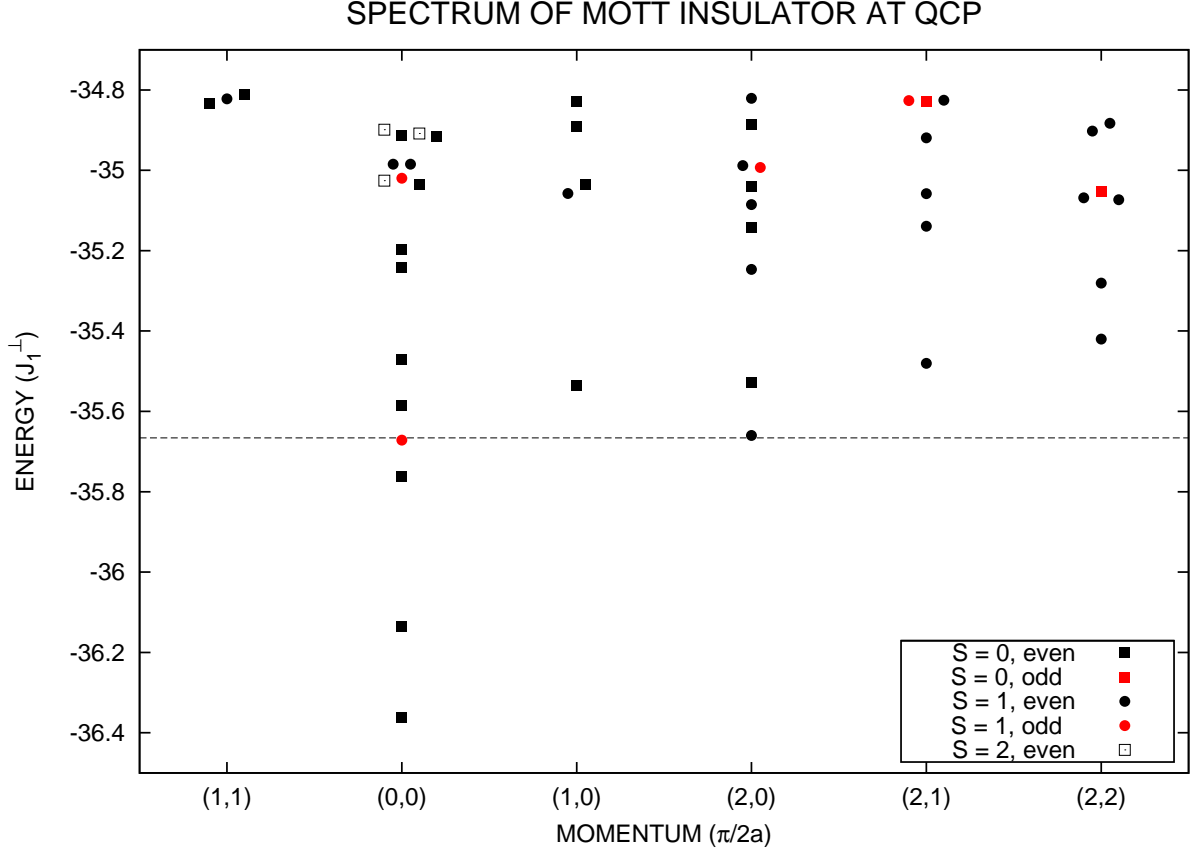


FIG. 3: The exact critical low-energy spectrum of the two-orbital Heisenberg model that corresponds to the two-orbital t - J model Eq. (1) over a 4×4 lattice (ref.²⁰). Heisenberg exchange coupling constants coincide with those in Fig. 1a, while the Hund coupling is $-J_{0c} = 1.35 J_1^\perp$. Black and red energy levels are respectively even and odd under $P_{d,\bar{d}}$. The horizontal dashed line marks the putative QCP: $\Delta_{cSDW} = 0$.

Hund coupling. Notice that the dispersion of low-energy spin-1 excitations in the exact critical spectrum, Fig. 3, is qualitatively similar to the critical spectrum predicted by the linear spin-wave approximation²⁰, Fig. 1a. The latter occurs at a critical Hund coupling $-J_{0c} = 2(J_1^\perp - J_1^\parallel) - 4J_2^\parallel = 0.8 J_1^\perp$ that is 40% smaller than the former exact result. Last, the linear spin-wave approximation and exact results over a 4×4 lattice of iron atoms indicate that the above QCP marks a second-order quantum phase transition³⁵ between a cSDW at strong Hund coupling and a hidden-order magnet (6) at weak Hund coupling. (See Appendix A and ref.²⁰.)

Two Holes. Figure 4 displays the low-energy spectrum of two holes roaming over a 4×4 lattice of spin-1 iron atoms under periodic boundary conditions. The t - J model parameters

are set to produce hole bands at zero 2D momentum for non-interacting electrons (Fig. 1c) and cSDW spin order via magnetic frustration when Hund's Rule is obeyed²²: $t_1^{\parallel} = -5J_1^{\perp}$, $t_1^{\perp}(\hat{\mathbf{x}}) = -2J_1^{\perp}$, $t_1^{\perp}(\hat{\mathbf{y}}) = +2J_1^{\perp}$, along with the previous Heisenberg exchange coupling constants. Further, the absence of next-nearest neighbor hopping imposes conventional particle-hole symmetry in the hole spectrum. It also turns off hybridization between holes in the d_{xz} and the d_{yz} orbitals. Next, the on-site hole-hole repulsion between the $d+$ and $d-$ orbitals is set to a large value $U'_0 = \frac{1}{4}J_0 + 1000 J_1^{\perp}$. Last, the ferromagnetic Hund's Rule exchange coupling constant is tuned to the critical value $J_0 = -2.25 J_1^{\perp}$, where true spin resonances at cSDW momenta that have even parity under orbital swap are degenerate with a hidden-order spin resonance at zero 2D momentum that has odd parity under orbital swap. This defines a putative quantum critical point that is realized at half filling in the limit of large electron spin²⁰ s_0 . (Cf. Figs. 1a,b and Fig. 3.) The critical Hund coupling at half filling and at large s_0 is considerably smaller: $-J_{0c} = 0.8 J_1^{\perp}$. The larger Hund coupling in the present case of two mobile holes is a result of the dominant intra-orbital hopping (t_1^{\parallel}) conspiring with hidden anti-ferromagnetic order ($\nearrow_{d-} \searrow_{d+}$) to form a hidden half metal state at weak Hund coupling²⁰⁻²².

It is important to notice the groundstate and the zero-momentum excited state that lie below the horizontal dashed line in Fig. 4. Their reflection parities are listed in Table II. Here, R_{xz} , R_{yz} and $R_{x'z}$ denote reflections about the xz plane, the yz plane, and about the $(x+y)z$ plane. The reflection parities indicate that the ground state is s -wave and that the excited state is d -wave. Figure 5 shows the evolution of the s -wave groundstate energy and of the d -wave excited-state energy with increasing Hund coupling. Notice how they merge at the putative QCP, yet avoid crossing. The difference in energy versus Hund coupling displays a prolonged inflection point there: $E_D - E_S \propto J_0 - J_{0c}$, with $-J_{0c} \cong 2.30 J_1^{\perp}$. It suggests a QCP for a single pair of holes in the two-orbital t - J model (1) at the thermodynamic limit that is consistent with the one predicted at half-filling by linear spin-wave theory about hidden magnetic order²⁰. Indeed, the QCP extracted from Fig. 5b is close to that specified by the degeneracy of the hidden spin-wave and the true spin-wave excitations. The latter is depicted by the horizontal dashed line in Fig. 4.

The inset to Fig. 5a shows the dependence of low-energy levels at zero net momentum on Hund coupling in the vicinity of the QCP. By contrast with the s/d -wave energy splitting, the edge of the particle-hole continuum in the exact two-hole spectrum at zero net momentum

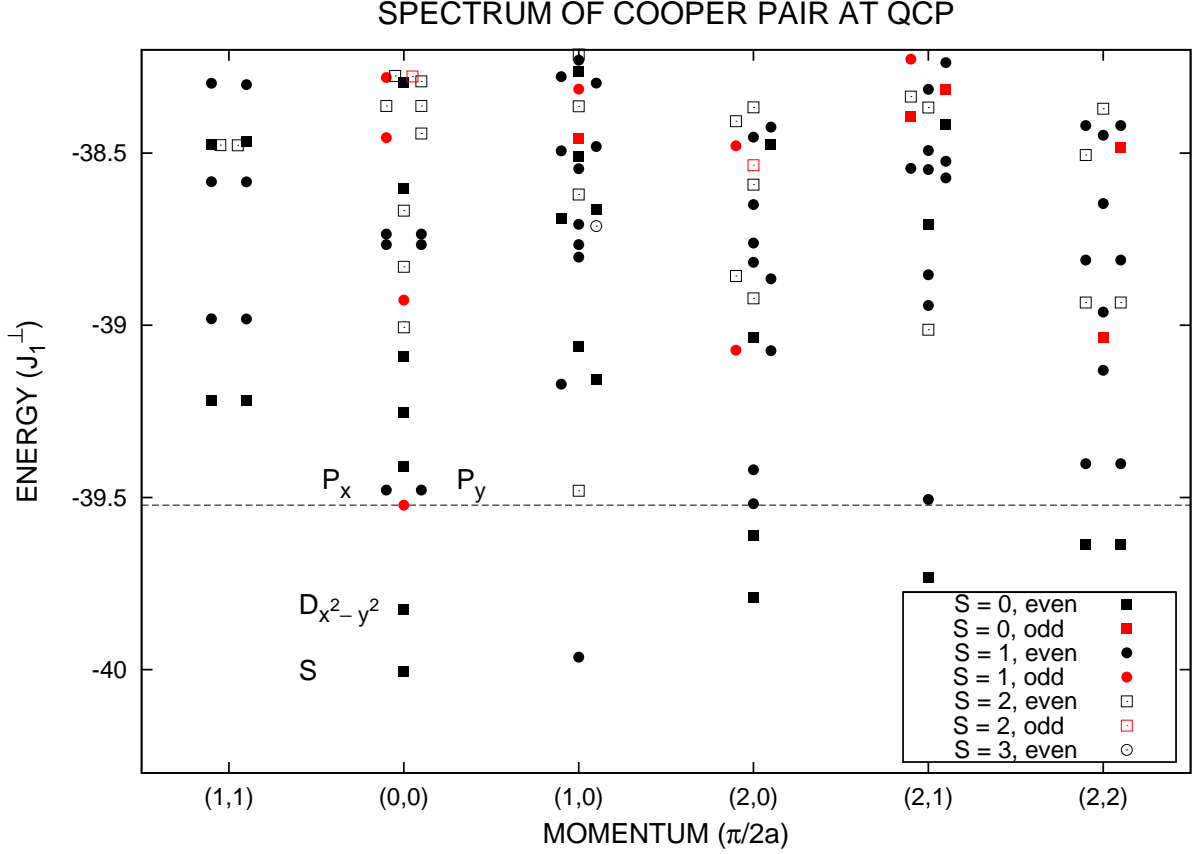


FIG. 4: The critical low-energy spectrum of the two-orbital t - J model, Eq. (1) plus the constant $\frac{1}{4}J_0(N_{\text{Fe}} - 2)$, for two holes roaming over a 4×4 lattice. Heisenberg exchange and hopping parameters coincide with those in Fig. 1. Hund coupling is at the critical value $-J_0 = 2.25 J_1^\perp$, while inter-orbital on-site repulsion is set to $U'_0 = \frac{1}{4}J_0 + 1000 J_1^\perp$. Black and red states are respectively even and odd under $P_{d,\bar{d}}$. Some points on the spectrum are artificially moved slightly off their quantized values along the momentum axis for the sake of clarity. The horizontal dashed line marks the putative QCP: $\Delta_{cSDW} = 0$.

does *not* collapse to the s -wave groundstate, nor to the d -wave excited state, as Hund coupling increases past the QCP. Instead, the QCP coincides with the gap maximum marked by the level crossing (dashed lines) in the inset to Fig. 5a. In other words, the quasi-particle gap (E_b) remains nonzero at the QCP.

no.	Hole-Pair State	R_{xz}	R_{yz}	$R_{x'z}$	$P_{d,\bar{d}}$	spin
0	S	+	+	+	+	0
1	$D_{x^2-y^2}$	+	+	-	+	0
2	hidden spinwave	-	-	-	-	1
3a	P_x	+	-	none	+	1
3b	P_y	-	+	none	+	1

TABLE II: Reflection parities, orbital-swap parity, and spin of low-energy hole-pair states with zero net momentum in order of increasing energy. (See Fig. 4.)

V. COOPER PAIRS AND COLLECTIVE EXCITATIONS

The low-energy spectrum for the two-orbital t - J model with two holes displayed by Fig. 4 features nearly degenerate s -wave and d -wave hole-pair bound states. Figure 5b strongly suggests that they become degenerate at a QCP in the thermodynamic limit. Below, we demonstrate that these states are the principal members of a family of Cooper pairs (8) characterized by a neutral spin-zero collective mode.

Singlet Pairs. The horizontal dashed line in Fig. 4 marks the degeneracy of the cSDW spin resonances with the hidden-order spin resonance at zero 2D momentum. At half filling, the same degeneracy occurs at a QCP that separates cSDW order from hidden magnetic order within the semi-classical approximation valid at large electron spin²⁰. The dashed horizontal line in Fig. 4 lies at the edge of a continuum of states with zero net momentum. Two bound states exist below the continuum at zero net momentum: an s -wave groundstate and a d -wave (second) excited state. The former is even under a physical reflection about the x - y diagonal that includes a swap of the d_{xz} and d_{yz} orbitals, while the latter is odd under it. (See Table II.) Figure 6 depicts the corresponding order parameters for superconductivity:

$$iF(k_0, \mathbf{k}) = \langle \Psi_{\text{Mott}} | \tilde{c}_\uparrow(k_0, \mathbf{k})^\dagger \tilde{c}_\downarrow(k_0, -\mathbf{k})^\dagger | \Psi_{\text{Cooper}} \rangle \quad (7)$$

times $\sqrt{2}$, with $\tilde{c}_s(k_0, \mathbf{k}) = \mathcal{N}^{-1/2} \sum_i \sum_{\alpha=0,1} e^{-i(k_0\alpha + \mathbf{k}\cdot\mathbf{r}_i)} \tilde{c}_{i,\alpha,s}$. Here, $\mathcal{N} = 32$ is two times the number of iron atoms, while the $d-$ and $d+$ orbitals α are enumerated by 0 and 1. The bonding and anti-bonding superpositions of these orbitals, $k_0 = 0$ and π , hence correspond to the d_{xz} and $-id_{yz}$ orbitals. Also, $\langle \Psi_{\text{Mott}} |$ denotes the critical antiferromagnetic state of the corresponding Heisenberg model²⁰ at $-J_{0c} = 1.35 J_1^\perp$. (See Fig. 3.) The groundstate is

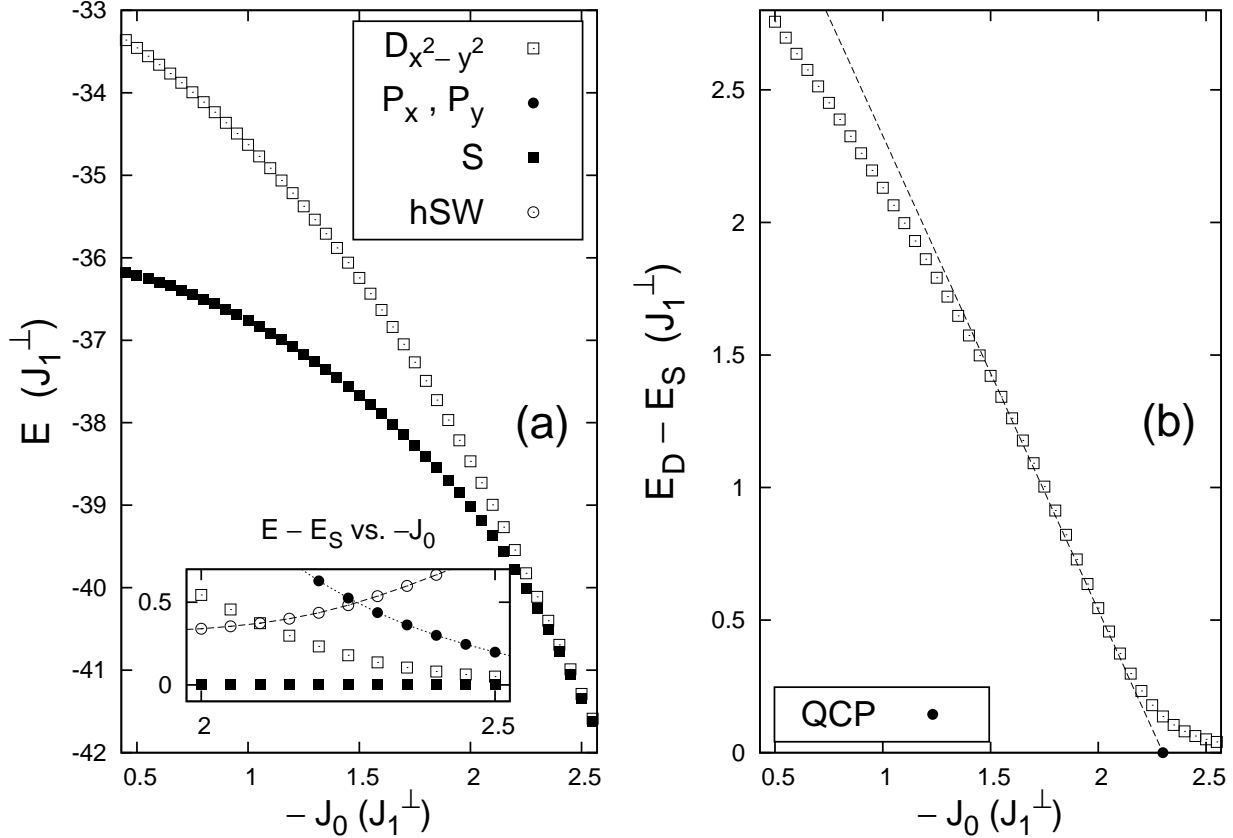


FIG. 5: (a) Exact energies for the groundstate s -wave pair state and for the first-excited d -wave pair state versus Hund coupling. (b) Energy splitting versus Hund coupling. The dashed line is a fit. Model parameters t and J coincide with those in Fig. 1.

primarily $|S^{+-}\rangle = \frac{1}{\sqrt{2}}|d_{yz}^{2(+-)}\rangle + \frac{1}{\sqrt{2}}|d_{xz}^{2(+-)}\rangle$, with some admixture of $|S^{++}\rangle = \frac{1}{\sqrt{2}}|d_{yz}^{2(++)}\rangle + \frac{1}{\sqrt{2}}|d_{xz}^{2(++)}\rangle$: $|S\rangle = (\cos\theta_0)|S^{+-}\rangle + (\sin\theta_0)|S^{++}\rangle$, where $\theta_0 = 27^\circ$. Here, $|d_{yz}^{2(+-)}\rangle$ and $|d_{xz}^{2(+-)}\rangle$ are singlet Cooper pairs restricted to each orbital, with equal and opposite values between the corresponding hole and emergent electron pockets, while $|d_{yz}^{2(++)}\rangle$ and $|d_{xz}^{2(++)}\rangle$ are the same, but with equal values at the corresponding hole and emergent electron pockets. The former are sketched in Fig. 1d (blue versus red), and they are defined in Table III. Figure 6 also shows that the first-excited pair state is $|D^{+-}\rangle = \frac{1}{\sqrt{2}}|d_{yz}^{2(+-)}\rangle - \frac{1}{\sqrt{2}}|d_{xz}^{2(+-)}\rangle$. The nature of the groundstate and first-excited pair states is correctly captured by a three-state model analyzed in Appendix B.

And what is the diameter of the s -wave and of the d -wave Cooper pairs identified in Fig. 4? An orbital trace, $iF(0, \mathbf{k}) - iF(\pi, \mathbf{k})$, of the principal S^{+-} component in the s -wave groundstate shown by Fig. 6 is approximated by $\cos(k_x a) + \cos(k_y a) + \cos(k_+ a) + \cos(k_- a)$,

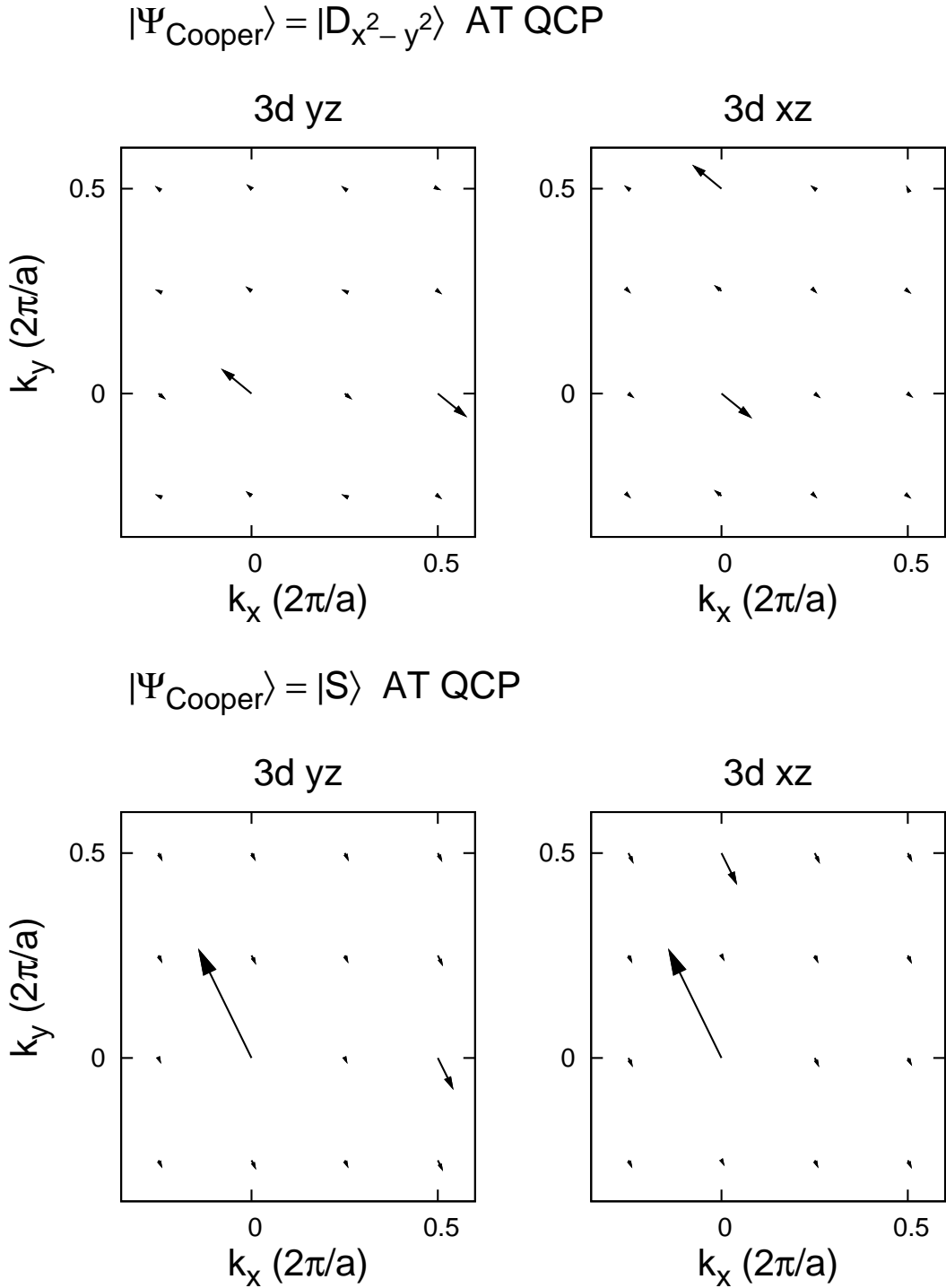


FIG. 6: The complex order parameter for superconductivity, $\sqrt{2}iF(k)$, of the s -wave groundstate and of the d -wave excited state in vector representation. It is symmetrized with respect to both reflections about the principal axes. Both the antiferromagnetic Mott insulator (Fig. 3) and the Cooper pair (Fig. 4) are at the QCP.

Cooper Pair	d_{yz} - d_{yz}	d_{xz} - d_{xz}
singlet $d_{yz}^{2(+-)}$	$(1 + \cos k_y a) \cos k_x a$	0
singlet $d_{xz}^{2(+-)}$	0	$(1 + \cos k_x a) \cos k_y a$

TABLE III: The pair amplitudes (7) of orbitally ordered states at the QCP.

where $k_{\pm} = k_x \pm k_y$, while an orbital trace of the D^{+-} pair state is approximated by $\cos(k_x a) - \cos(k_y a)$. The S^{+-} pair state is then approximately the superposition of all nearest neighbor and next-nearest neighbor pairs, while the D^{+-} pair state is approximately the difference of all x -axis-aligned and of all y -axis-aligned nearest neighbor pairs. Notice that these traces are consistent with the component pair wavefunctions per orbital listed in Table III. The s -wave and d -wave bound states each thus fit in a unit cell. This implies that the 4×4 lattice studied here is sufficiently big. Macroscopic condensation into one of these pair states then necessarily results in a strong-coupling superconductor⁴²⁻⁴⁴, possibly of the short-range RVB type⁴⁵.

Orbital Pair Oscillations. Following refs.^{29, 30}, and³¹, an internal Josephson effect links the s -wave and d -wave pair states identified by Fig. 6, where holes condense into a dynamical Cooper pair state of the form $\frac{1}{\sqrt{2}}e^{i\phi(d_{yz})}|d_{yz}^{2(+-)}\rangle + \frac{1}{\sqrt{2}}e^{i\phi(d_{xz})}|d_{xz}^{2(+-)}\rangle$. Here, we have ignored the relatively small S^{++} contribution of the s -wave pair state evident in Fig. 6. A three-state model of the Cooper pairs in question finds that this is possible sufficiently near the QCP. (See Appendix B.) Notice that the probability of finding a pair of holes in either a $|d_{yz}^{2(+-)}\rangle$ state or in a $|d_{xz}^{2(+-)}\rangle$ state is equal to 1/2 for the proposed pair wavefunction, as demanded by 2D isotropy. An explicit Bardeen-Cooper-Schrieffer (BCS) wave function for the macroscopic superconductor that projects out double occupancy of electrons⁴⁵ per iron site-orbital as well as double-occupancy of holes per iron atom can be written down⁴⁶. It has the form³⁰ $|\Psi_{pBCS}\rangle = \sum_{N=0}^{\infty} c_N e^{iN\phi} |\Psi_N\rangle$, where $|\Psi_N\rangle$ represents $2N$ mobile holes condensed into the Cooper pair

$$|\psi_{J'}(\phi_-)\rangle = \frac{e^{+i\phi_-/2}}{\sqrt{2}}|d_{yz}^{2(+-)}\rangle + \frac{e^{-i\phi_-/2}}{\sqrt{2}}|d_{xz}^{2(+-)}\rangle, \quad (8)$$

and where c_N are real constants that are sharply peaked at the mean number of pairs. Above, $\phi_- = \phi(d_{yz}) - \phi(d_{xz})$ and $\phi = \frac{1}{2}[\phi(d_{yz}) + \phi(d_{xz})]$. Orbital order $N_- = N(d_{yz}) - N(d_{xz})$ is sharply peaked at zero per the binomial distribution at macroscopically large⁴⁷ $N =$

$N(d_{yz})+N(d_{xz})$. Here, $N(o)$ counts the number of Cooper pairs in orbital o . The phase of the orbitally ordered pairs, $\phi(o)$, is canonically conjugate to it. We therefore have commutation relations $[\frac{1}{2}\phi_-, N_-] = i = [\phi, N]$. The remaining commutators vanish.

An internal Josephson effect between the two species of orbitally ordered Cooper pairs, $|d_{yz}^{2(+)}\rangle$ and $|d_{xz}^{2(+)}\rangle$, is then predicted by the following hydrodynamic Hamiltonian:

$$H_{\text{orb}} = V \left[\frac{1}{2\chi_{\text{orb}}} \left(\frac{N_-}{V} \right)^2 - \frac{\mu_-}{2} \frac{N_-}{V} - e_{J'} \cos(\phi_-) \right], \quad (9)$$

where $\mu_- = \mu(d_{yz}) - \mu(d_{xz})$ is the difference in chemical potential between the two orbitals. Also, V denotes the area of an iron-pnictide layer. Above, χ_{orb} is the susceptibility for orbital order of the Cooper pairs at zero temperature. It attains the normal-state value equal to one half the density of states in the hydrodynamic regime⁴⁸. Also, $e_{J'}$ is one half the difference in condensation energy density between the S^{+-} state and the D^{+-} state. It is given by $e_{J'} \cong \frac{1}{2}(N/V)(E_D - E_S)$ in the regime of local Cooper pairs. Notice from (8) and (9) that the equilibrium groundstate is S^{+-} , and that it shows no orbital order: $\phi_- = 0$ and $N_- = 0$ at $\mu_- = 0$. The D^{+-} pair state, on the contrary, is in unstable equilibrium: $\phi_- = \pi$ and $N_- = 0$ at $\mu_- = 0$. Hydrodynamic equilibrium is therefore consistent with the s -wave groundstate found by the previous exact calculations at subcritical Hund coupling. (See Fig. 5.) Orbital ordering of the macroscopic superconductor is then governed by standard dynamical equations³⁰: $\hbar\frac{1}{2}\dot{\phi}_- = \chi_{\text{orb}}^{-1}(N_-/V) - \frac{1}{2}\mu_-$ and $\hbar\frac{1}{2}\dot{N}_-/V = -e_{J'} \sin(\phi_-)$, while N , ϕ and $\mu = \frac{1}{2}[\mu(d_{yz}) + \mu(d_{xz})]$ remain constant.

The previous dynamical equations imply small oscillations in N_- and ϕ_- about zero that are 90° out of phase, at a natural frequency $\omega_{J'}$ that is related to the internal Josephson tunneling by³¹ $(\hbar\omega_{J'})^2 = 4e_{J'}/\chi_{\text{orb}}$. The collective oscillation is undamped as long as it lies inside the quasi-particle energy gap: $\hbar\omega_{J'} < E_b$. Figure 5b suggests that $\omega_{J'}$ collapses to zero at the QCP and/or at half-filling as the product $(N/V)^{1/2} \cdot \text{Re}(J_0 - J_{0c})^{1/2}$. Unlike the s/d -wave energy splitting in the exact spectrum, Fig. 4, the energy gap that separates the S^{+-} groundstate from the edge of the particle-hole continuum does *not* tend to zero at the QCP. (See the dashed lines in the inset to Fig. 5a.) The neutral spin-0 collective mode is hence observable in the quantum critical region or near half filling. Last, orthorhombic shear strain couples to this internal Josephson effect through the electron-phonon interaction^{33,34}: $\frac{1}{2}\mu_- = \Xi_{u'}\frac{1}{2}(\partial u_x/\partial x - \partial u_y/\partial y)$, where $\Xi_{u'}$ is a deformation potential, and where \mathbf{u} is the displacement field of the iron atoms. Level repulsion between the spectrum of orthorhombic

phonons and the above neutral spin-0 collective mode is then possible if the Debye frequency in the iron-pnictide superconductor is larger than ω_J . The Debye frequency is typically comparable to the energy gap in iron-pnictide superconductors⁴⁹. Hence, the collective mode couples strongly to such orthorhombic phonons in the quantum critical region or near half filling.

Triplet Pairs. The low-energy spectrum for two holes shown by Fig. 4 also contains a degenerate pair of spin-1 states with no net momentum that lie at the edge of the continuum of states. One is a P_x state, with even parity under a reflection about the x axis and odd parity under a reflection about the y axis, while the other is a P_y state, with these parities reversed. (See Table II.) This symmetry along with orbital order is revealed by the order parameter for superconductivity (7) of the P_x state, for example: $\sqrt{2}iF(k_0, \mathbf{k}) \cong 0.056 \sin(k_x a)$ for k_y near 0 in the d_{yz} - d_{yz} pair channel, and $\sqrt{2}iF(k_0, \mathbf{k}) \cong 0$ otherwise. Here, $\sqrt{2}iF(k)$ has been symmetrized with respect to a reflection about the x axis. Now notice the spin-1 state at momentum $\hbar(\pi/2a)\hat{x}$ in Fig. 4 that is nearly degenerate with the groundstate. We propose that the former P states are degenerate triplet Cooper pairs, and that the latter spin-1 state is a remnant of the corresponding Leggett mode³². Note that the possibility of an orbital singlet is excluded here. At the QCP, it coincides instead with the hidden-order spin resonance at zero 2D momentum. (See the “red” states in Fig. 4.)

VI. DISCUSSION

Below, we describe the emergent nature of the S^{+-} Cooper pair exhibited by Fig. 6 and the implications of the QCP shown by Fig. 5b on the collective mode. We also argue that the d -wave pair state remains higher in energy than the s -wave pair state at dilute concentrations of charge carriers, and we survey the nature of the two-hole spectrum, Fig. 4, at net momentum.

A. Lifshitz Transition versus Quantum Critical Point

Schwinger-boson-slave-fermion meanfield theory for the hidden half-metal state predicts that the emergent electron bands shown by Fig. 2b first cross the Fermi level at cSDW momenta when the energy difference Δ_{cSDW} between cSDW spinwaves and the hidden-

order spinwave at zero 2D momentum vanishes²¹. (See Fig. 2a.) It therefore predicts that the former Lifshitz transition coincides with the latter QCP shown by Fig. 1a at half filling. Exact results on a 4×4 lattice of iron atoms find that the putative QCP ($\Delta_{cSDW} = 0$) occurs at Hund coupling $-J_{0c} = 1.35 J_1^\perp$ in the absence of mobile holes (Fig. 3), while the Lifshitz transition occurs at $-J_{0c} = -1.73 J_1^\perp$ in the case of one mobile hole²². In the case of two mobile holes, the putative QCP, which is marked by the dashed horizontal line in Fig. 4, lies at the critical Hund coupling $-J_{0c} = 2.25 J_1^\perp$. The monotonic increase of $-J_{0c}$ with the mobile hole concentration per orbital x is consistent with the linear increase (5) of $-J_{0c}$ with x obtained within the meanfield approximation²¹. Finally, the dependence of the energy splitting between the S^{+-} hole-pair groundstate and the D^{+-} hole-pair excited state on Hund coupling shown by Fig. 5b for a 4×4 lattice of spin-1 iron atoms suggests a QCP in the thermodynamic limit at which these states become degenerate. It occurs at $-J_{0c} = 2.30 J_1^\perp$, which is close to the putative QCP. The $d_{yz}^{2(+-)}$ and $d_{xz}^{2(+-)}$ Cooper pairs that are listed in Table III become degenerate boundstates in such case, however. This strongly suggests that the latter QCP for a single pair of mobile holes coincides with the Lifshitz transition exhibited by one mobile hole and predicted by meanfield theory²². Comparison with Fig. 6 and the inset to Fig. 5a further also strongly suggests remnant Cooper pairs of opposite sign on the emergent electron bands that lie above the Fermi level at subcritical Hund coupling. A similar prediction was made recently by Bang on the basis of a phenomenological model for a heavily hole-doped iron-pnictide superconductor³⁶.

Now recall that the hydrodynamic Hamiltonian (9) predicts a spin-0 collective d -wave oscillation of the S^{+-} Cooper pair at long wavelength. The s/d -wave energy-splitting density in a macroscopic superconductor at a dilute number of hole pairs N is $2e_{J'} \cong (N/V)(E_D - E_S)$. Using the dependence $E_D - E_S \propto \max(0, J_0 - J_{0c})$ for the s/d -wave energy splitting suggested by Fig. 5b yields the following expression for the dependence of the excitation energy of the spin-0 collective mode: $\hbar\omega_{J'} \propto (N/V)^{1/2} \cdot \text{Re}(J_0 - J_{0c})^{1/2}$. It collapses to zero at the QCP and/or at half-filling. This result also implies that $\hbar\omega_{J'} = 0$ at super-critical Hund coupling, where $\Delta_{cSDW} = 0$. The groundstate S^{+-} Cooper pair shown in Fig. 4, hence, is stable *only* at subcritical Hund coupling. More generally, the barrier for internal Josephson tunneling $e_{J'}$ vanishes at the QCP. In such case, the relative phase ϕ_- winds freely, which destroys internal phase coherence in the Cooper pair wavefunction (8). The quantum critical state³⁵ at the QCP therefore shows net superconducting phase coherence

at long range, which couples to electric charge, but it shows no internal phase coherence that can discriminate between s , d , or $s + id$ pair symmetry, for example, at long range. [Cf. Eq. (11).] The previous exact results for two holes in the two-orbital t - J model (1) confirm the collapse of the collective-mode spectrum to zero excitation energy predicted above, but at short wavelength. In particular, the groundstate spin-0 energy levels at cSDW momenta shown in Fig. 4 fall below the energy level of the s -wave Cooper pair as Hund coupling increases past the QCP.

B. Local Cooper Pairs

Figure 5 strongly suggests that the d -wave Cooper pair remains higher in energy than the groundstate s -wave Cooper pair, despite the fact that the energy splitting tends to zero at the QCP. Does this ranking in energy persist in the thermodynamic limit at a dilute concentration of charge carriers? And does long-range phase coherence prevail in such case? We answer these two questions affirmatively below on the basis of the local nature of the Cooper pairs.

The exact results shown in Fig. 6 for the s -wave and d -wave pair wave functions suggest the component wavefunctions per orbital that are listed in Table III. They are short range and extend at most an iron-pnictide lattice constant $a' = \sqrt{2}a$. Following the results of the three-state model introduced in Appendix B, the $d_{yz}^{2(+)}$ and $d_{xz}^{2(+)}$ pairs primarily experience a diagonal Hamiltonian matrix element $-E_b$ and an off-diagonal Hamiltonian matrix element $-\mathcal{T}_0$ at the QCP. They account, respectively, for the binding and for the internal Josephson tunneling between the component pair states. A positive sign for the tunneling parameter \mathcal{T}_0 yields an energy splitting between an s -wave groundstate and a d -wave excited state. Trial BCS wavefunctions for S^{+-} and D^{+-} pairs (8) that project out double-occupancy at an iron site per $d\pm$ orbital exhibit promising energies at half filling⁴⁶. Following Leggett's results for unprojected BCS states^{43,44}, it is plausible then to assume that the groundstate at a dilute concentration of charge carriers is a Bose condensate of local S^{+-} Cooper pairs that shows long-range phase coherence.

This picture of a Bose condensate of local Cooper pairs is encoded by the Ginzburg-Landau free-energy functional to lowest order,

$$\mathcal{F}_{cond}^{(2)} = |\nabla\Psi|^2/2m_* - E_b|\Psi|^2 - \mathcal{T}_0(\Psi_x\Psi_y^* + \Psi_x^*\Psi_y), \quad (10)$$

where $\Psi = (\Psi_x, \Psi_y)$ is the two-component order parameter for $d_{yz}^{2(+-)}$ and $d_{xz}^{2(+-)}$ pairing, respectively. Above, m_* is the effective mass of a pair of holes. The coherence length extracted from (10) is therefore $\xi_0 = (2m_*E_b)^{-1/2}$. Taking $E_b \cong 0.4 J_1^\perp$ for the binding energy from the spectrum displayed by Fig. 4 and $m_*^{-1} = |t_1^\parallel|a^2$ for the inverse effective mass yields the estimate $\xi_0 \cong (|t_1^\parallel|/0.8J_1^\perp)^{1/2}a \cong 0.70$ nm for the coherence length in iron-based superconductors. Here, hopping coincides with Fig. 1c, and $a = 2.8 \text{ \AA}$ is the intra-layer Fe-Fe distance in optimally hole-doped (Ba,K)Fe₂As₂⁵⁰. Experimental determinations of the upper-critical magnetic field along the c axis in the hole-doped series of iron-pnictide superconductors Ba_{1-x}K_xFe₂As₂ find steep slopes versus temperature at T_c near optimal doping^{51,52}. In particular, determinations of the irreversibility field along the c axis at $x \cong 0.4$ find that the product of this slope with T_c is⁵³ $H_1 = -T_c(dH_{c2}/dT)|_c = 2.5$ MOe. Substitution into the formula $\xi_1 = (\Phi_0/2\pi H_1)^{1/2}$ for the Ginzburg-Landau coherence length, with the magnetic flux quantum $\Phi_0 = 2.07 \times 10^{-7}$ G cm², yields the estimate $\xi_1 = 1.16$ nm. It is comparable to the previous estimate for the coherence length based on local Cooper pairs.

C. Dispersion of Two-Hole Spectrum

The nature of the low-energy spectrum displayed by Fig. 4 for a pair of holes roaming over a 4×4 lattice of spin-1 iron atoms (1) with *net* 2D momentum further corroborates the identification of the groundstate at zero 2D momentum as a S^{+-} Cooper pair. In particular, the groundstate at cSDW wavenumber $(\pi/a)\hat{\mathbf{x}}$ is spin-0, and it is even and odd under reflections about the x axis and the y axis, respectively. It is therefore consistent with a moving $|d_{yz}^{2(+-)}\rangle$ Cooper pair state: $\sin[(\pi/2a)(x_1 + x_2)]\langle 1, 2|d_{yz}^{2(+-)}\rangle$. Indeed, a direct computation of the pair amplitude (7) finds that it is proportional to $\sin k_x a$ at $k_y = 0$ in the d_{yz} - d_{yz} pair channel, while it is approximately zero otherwise. (Cf. Table III.) Next, the lowest-energy spin-1 state in Fig. 4 at this cSDW momentum is the critical cSDW spin resonance, which can be interpreted as a pair excitation of the S^{+-} groundstate^{54,55}. It has even parity under a reflection about the x axis, as well as about the y axis. The spin resonance at wavenumber $(\pi/a)\hat{\mathbf{x}}$ can therefore also be interpreted as a moving P_x triplet Cooper pair: $\sin[(\pi/2a)(x_1 + x_2)]\langle 1, 2|P_x\rangle$. Also, both the first-excited spin-0 and spin-1 states at wavenumber $(\pi/a)\hat{\mathbf{x}}$ are odd and even under reflections about the x axis and the

y axis, respectively. They may therefore be interpreted as particle-hole excitations of the groundstate S^{+-} Cooper pair. Further, the spin-0 and spin-1 groundstates at wavenumbers $(1, 1)$ and $(2, 2)$ in units of $\pi/2a$ share the same parity under a true reflection about the x - y diagonal, which includes swap of the d_{xz} and d_{yz} orbitals. In particular, the even and odd parity states are degenerate per spin. We therefore also interpret these low-lying states as particle-hole excitations of the groundstate S^{+-} Cooper pair. Finally, both the spin-0 and spin-1 groundstates at momentum $(2, 1)$ in Fig. 4 are even under a reflection about the y axis. The weak dispersion in energy per spin at nearby momenta suggests that the former is a spin-0 collective excitation of the groundstate S^{+-} Cooper pair and that the latter is a spin resonance of the same.

VII. SUMMARY AND CONCLUSIONS

We have found groundstate S^{+-} and excited-state D^{+-} Cooper pairs near a QCP where they become degenerate in a local-moment model for iron-based superconductors. Such Cooper pairing instabilities were predicted previously for iron-pnictide superconductors on the basis of perturbative spin-fluctuation exchange⁷. In the present local-moment model, however, the S^{+-} and D^{+-} Cooper pairs are respectively bonding and anti-bonding superpositions of orbitally ordered Cooper pairs that alternate in sign between hole and electron Fermi surfaces. With the exception of d_{xy} orbital character at the tips of the electron pockets²⁸, this result is consistent with the s -wave and d -wave solutions to the gap equation reported by Graser et al. in ref.⁸, which again invokes spin-fluctuation exchange, but within the random-phase approximation. Note that the binding energy of the s -wave singlet pair groundstate at the QCP shown in Fig. 4 implies a gap $E_b = 0.4 J_1^\perp$. Also, the inset to Fig. 5a indicates that this quasi-particle gap does *not* collapse to zero at the QCP. Taking a value of $J_1^\perp \sim 120$ meV from a fit to spin-wave spectra in iron-pnictide materials based on the corresponding two-orbital Heisenberg model (Fig. 1a and ref.²⁰) then yields a gap $E_b \sim 50$ meV. It is roughly consistent with the upper bound for the spin-resonance energy in iron-pnictide superconductors⁹, and it is consistent with high-temperature superconductivity.

Our focus on the degenerate d_{xz} and d_{yz} orbitals that feature prominently in iron superconductors reveals that the S^{+-} and D^{+-} bound pair states are linked by a collective excitation within a larger family of $s + id$ pair states (8). Observe, in particular, that such

pair wavefunctions can be re-expressed as

$$|\psi_{J'}(\phi_-)\rangle = (\cos \frac{1}{2}\phi_-)|S^{+-}\rangle + i(\sin \frac{1}{2}\phi_-)|D^{+-}\rangle. \quad (11)$$

The stable s -wave state notably passes through the $s + id$ state on route to the unstable d -wave state⁵⁶. Previously, Scalapino and Devereaux predicted a related d -wave exciton for the S^{+-} state at weak coupling⁵⁷, with the important distinction that they required nested electron-type Fermi surface pockets at cSDW momenta. Recent studies of Raman spectroscopy in the optimally hole-doped iron-pnictide superconductor $\text{Ba}_{0.6}\text{K}_{0.4}\text{Fe}_2\text{As}_2$ report experimental evidence for an in-gap collective mode^{37,38} consistent with the s -to- d -wave pair excitation identified here and in ref.⁵⁷. ARPES demonstrates that the electron pockets at cSDW momenta lie below the Fermi level at optimal doping^{3,4,11}. Within the present theory, optimal doping corresponds to super-critical Hund coupling, at which the frequency $\omega_{J'}$ of the collective mode has collapsed to a small value. The present theory predicts, however, that the collective mode persists at the Lifshitz transition, where the electron Fermi surface pockets vanish, and that the collective oscillation frequency has a similarly small value there. On this basis, we therefore predict that the s -to- d -wave collective mode observed in $\text{Ba}_{1-x}\text{K}_x\text{Fe}_2\text{As}_2$ at optimal doping^{37,38} will also be observed at higher doping near the Lifshitz transition^{10,15,16}.

Acknowledgments

The author thanks Xing-Jiang Zhou, Peter Hirschfeld, Thomas Maier, Paolo Zanardi and Stephan Haas for valuable discussions. He also thanks Brent Andersen, Richard Roberts and Timothy Sell for technical help with the use of the virtual shared-memory cluster (Lancer) at the AFRL DoD Supercomputing Resource Center. This work was completed in part during the 2014 program on “Magnetism, Bad Metals and Superconductivity: Iron Pnictides and Beyond” held at the Kavli Institute for Theoretical Physics, with partial support from the National Science Foundation (NSF) under grant no. PHY11-25915. This work was also supported in part by the US Air Force Office of Scientific Research under grant no. FA9550-13-1-0118 and by the NSF PREM program under grant no. DMR-1523588.

Appendix A: Quantum Critical Point at Half Filling

Near cSDW wavenumbers $\mathbf{Q}_{cSDW} = (\pi/a)\hat{\mathbf{x}}$ and $(\pi/a)\hat{\mathbf{y}}$, and in the absence of mobile holes, the spin-wave spectrum for the two-orbital t - J model (1) disperses anisotropically as

$$\omega(\mathbf{k}) = [\Delta_{cSDW}^2 + v_l^2(k_l - \pi/a)^2 + v_t^2 k_t^2]^{1/2} \quad (\text{A1})$$

within the semi-classical approximation about hidden magnetic order, $\nearrow_{d-} \searrow_{d+}$, at large electron spin²⁰, $s_0 \rightarrow \infty$. Here, k_l and k_t denote the components of wavenumber \mathbf{k} that are parallel and perpendicular to \mathbf{Q}_{cSDW} . Above, the spin gap at \mathbf{Q}_{cSDW} collapses to zero at the QCP as

$$\Delta_{cSDW} = (2s_0)[(4J_2^\perp - J_{0c})(J_0 - J_{0c})]^{1/2}, \quad (\text{A2})$$

while the longitudinal spin-wave velocity v_l and the anisotropy parameter v_l/v_t coincide with the values

$$v_0 = 2s_0 a [(J_1^\perp - J_1^\parallel + 2J_2^\perp - 2J_2^\parallel) \cdot (\frac{1}{2}J_0 + 2J_1^\perp + 2J_2^\perp)]^{1/2} \quad (\text{A3})$$

and

$$\gamma_0 = \left(\frac{2J_2^\parallel + 2J_2^\perp + J_1^\parallel + J_1^\perp}{2J_2^\parallel + 2J_2^\perp - J_1^\parallel - J_1^\perp} \right)^{1/2} \quad (\text{A4})$$

at criticality. The hidden-order phase is stable at weak Hund coupling, $-J_0 < -J_{0c}$, with $-J_{0c} = 2(J_1^\perp - J_1^\parallel) - 4J_2^\parallel$. The correlation length for cSDW order, $\xi_{cSDW} = v_l/\Delta_{cSDW}$, therefore diverges as $(J_0 - J_{0c})^{-1/2}$ at the QCP within the linear spin-wave approximation²⁰. It implies a second-order quantum phase transition³⁵, with critical exponents $\nu_{cSDW} = 1/2$ and $z_{cSDW} = 1$. Exact results for the same two-orbital Heisenberg model over a 4×4 lattice of iron atoms yield that the square of the hidden-order moment and the square of the cSDW-order moment dove-tail at the QCP²⁰. This also suggests a second-order quantum phase transition at the QCP in the thermodynamic limit.

At the long-wavelength limit, the spin-wave spectrum follows $\omega(\mathbf{k}) = v_0|\mathbf{k}|$ in the hidden-order phase within the semi-classical approximation. It has no spectral weight in the true spin channel, however. (See Figs. 1a,b.)

Appendix B: Three-State Model

The lowest-energy pair states in the two-orbital t - J model at the QCP shown by the spectrum in Fig. 4 can be described by the following effective Hamiltonian in the reduced

Hilbert space composed of the pair states $|x\rangle = |d_{yz}^{2(+-)}\rangle$, $|y\rangle = |d_{xz}^{2(+-)}\rangle$, and $|z\rangle = |S^{++}\rangle$:

$$H_{pair} = \begin{pmatrix} -E_b & -\mathcal{T}_0 & -\mathcal{T}_1 \\ -\mathcal{T}_0 & -E_b & -\mathcal{T}_1 \\ -\mathcal{T}_1 & -\mathcal{T}_1 & E_z \end{pmatrix}. \quad (\text{B1})$$

Above, $E_b > 0$ is the binding energy of the degenerate pair states $d_{yz}^{2(+-)}$ and $d_{xz}^{2(+-)}$, $E_z > 0$ is the energy of the S^{++} Cooper pair, and \mathcal{T}_0 and \mathcal{T}_1 are positive and real hybridization matrix elements, respectively, among the three pair states. Zero energy is set by the edge of the continuum. The eigenstates of (B1) can be easily found. They have the form

$$\begin{aligned} |0\rangle &= (\cos \theta_0)|S^{+-}\rangle + (\sin \theta_0)|S^{++}\rangle, \\ |1\rangle &= |D^{+-}\rangle, \\ |2\rangle &= -(\sin \theta_0)|S^{+-}\rangle + (\cos \theta_0)|S^{++}\rangle, \end{aligned} \quad (\text{B2})$$

where above we call $|S^{+-}\rangle = \frac{1}{\sqrt{2}}|d_{yz}^{2(+-)}\rangle + \frac{1}{\sqrt{2}}|d_{xz}^{2(+-)}\rangle$ and $|D^{+-}\rangle = \frac{1}{\sqrt{2}}|d_{yz}^{2(+-)}\rangle - \frac{1}{\sqrt{2}}|d_{xz}^{2(+-)}\rangle$.

Application of H_{pair} yields energy eigenvalues of the form

$$\begin{aligned} E_0 &= -E_b - \mathcal{T}_0 - \epsilon_0, \\ E_1 &= -E_b + \mathcal{T}_0, \\ E_2 &= E_z + \epsilon_0. \end{aligned} \quad (\text{B3})$$

Above, θ_0 is set by

$$\tan \theta_0 = (\text{sgn } \mathcal{T}_1) \sqrt{\left(\frac{\mathcal{T}_0 + \delta E}{2^{3/2}\mathcal{T}_1}\right)^2 + 1} - \frac{\mathcal{T}_0 + \delta E}{2^{3/2}\mathcal{T}_1}, \quad (\text{B4})$$

where $\delta E = E_z + E_b$ is the energy difference between the S^{++} pair state and the degenerate Cooper pairs $d_{yz}^{2(+-)}$ and $d_{xz}^{2(+-)}$. Also, $\epsilon_0 = 2^{1/2}\mathcal{T}_1 \tan \theta_0$ is a level-repulsion energy.

We shall now assume that both \mathcal{T}_0 and \mathcal{T}_1 tend to zero at the QCP. This yields the approximations

$$\theta_0 \cong 2^{1/2}\mathcal{T}_1/\delta E, \quad (\text{B5})$$

$$\epsilon_0 \cong 2\mathcal{T}_1^2/\delta E \quad (\text{B6})$$

for the mixing angle and for the energy-level repulsion near the QCP, at $\mathcal{T}_0, \mathcal{T}_1 \ll \delta E$. Inspection of (B2) and (B3) yields that they are negligibly small in that critical region.

-
- ¹ D.J. Singh and M.-H. Du, Phys. Rev. Lett. **100**, 237003 (2008).
 - ² J. Dong, H. J. Zhang, G. Xu, Z. Li, G. Li, W. Z. Hu, D. Wu, G. F. Chen, X. Dai, J. L. Luo, Z. Fang, N. L. Wang, Euro. Phys. Lett. **83**, 27006 (2008).
 - ³ H. Ding, P. Richard, K. Nakayama, T. Sugawara, T. Arakane, Y. Sekiba, A. Takayama, S. Souma, T. Sato, T. Takahashi, Z. Wang, X. Dai, Z. Fang, G.F. Chen, J.L. Luo and N.L. Wang, Euro. Phys. Lett. **83**, 47001 (2008).
 - ⁴ K. Nakayama, T. Sato, P. Richard, Y.-M. Xu, Y. Sekiba, S. Souma, G.F. Chen, J.L. Luo, N.L. Wang, H. Ding, Euro. Phys. Lett. **85**, 67002 (2009).
 - ⁵ I.I. Mazin, D.J. Singh, M.D. Johannes, and M.H. Du, Phys. Rev. Lett. **101**, 057003 (2008).
 - ⁶ K. Kuroki, S. Onari, R. Arita, H. Usui, Y. Tanaka, H. Kontani, and H. Aoki, Phys. Rev. Lett. **101**, 087004 (2008).
 - ⁷ F. Wang, H. Zhai, Y. Ran, A. Vishwanath, and D.-H. Lee, Phys. Rev. Lett. **102**, 047005 (2009).
 - ⁸ S. Graser, T.A. Maier, P.J. Hirschfeld, and D.J. Scalapino, New J. Phys. **11**, 025016 (2009).
 - ⁹ J. Paglione and R.L. Greene, Nature Physics **6**, 645 (2010).
 - ¹⁰ S.L. Bud'ko, M. Sturza, D.Y. Chung, M.G. Kanatzidis and P.C. Canfield, Phys. Rev. B **87**, 100509(R) (2013).
 - ¹¹ K. Nakayama, T. Sato, P. Richard, Y.-M. Xu, T. Kawahara, K. Umezawa, T. Qian, M. Neupane, G.F. Chen, H. Ding, and T. Takahashi, Phys. Rev. B **83**, 020501(R) (2011).
 - ¹² K. Hashimoto, T. Shibauchi, S. Kasahara, K. Ikada, S. Tonegawa, T. Kato, R. Okazaki, C.J. van der Beek, M. Konczykowski, H. Takeya, K.Hirata, T. Terashima and Y. Matsuda, Phys. Rev. Lett. **102**, 207001 (2009).
 - ¹³ X.G. Luo, M.A. Tanatar, J.-Ph. Reid, H. Shakeripour, N. Doiron-Leyraud, N. Ni, S.L. Bud'ko, P.C. Canfield, H. Luo, Z. Wang, H.-H. Wen, R. Prozorov and L. Taillefer, Phys. Rev. B **80**, 140503(R) (2009).
 - ¹⁴ T. Sato, K. Nakayama, Y. Sekiba, P. Richard, Y.-M. Xu, S. Souma, T. Takahashi, G.F. Chen, J.L. Luo, N.L. Wang and H. Ding, Phys. Rev. Lett. **103**, 047002 (2009).
 - ¹⁵ W. Malaeb, T. Shimojima, Y. Ishida, K. Okazaki, Y. Ota, K. Ohgushi, K. Kihou, T. Saito,

- C.H. Lee, S. Ishida, M. Nakajima, S. Uchida, H. Fukazawa, Y. Kohori, A. Iyo, H. Eisaki, C.-T. Chen, S. Watanabe, H. Ikeda, and S. Shin, *Phys. Rev. B* **86**, 165117 (2012).
- ¹⁶ H. Hodovanets, Y. Liu, A. Jesche, S. Ran, E.D. Mun, T.A. Lograsso, S.L. Bud'ko and P.C. Canfield, *Phys. Rev. B* **89**, 224517 (2014).
- ¹⁷ S.N. Khan and D.D. Johnson, *Phys. Rev. Lett.* **112**, 156401 (2014).
- ¹⁸ Q. Si and E. Abrahams, *Phys. Rev. Lett.* **101**, 076401 (2008).
- ¹⁹ J.P. Rodriguez and E.H. Rezayi, *Phys. Rev. Lett.* **103**, 097204 (2009).
- ²⁰ J.P. Rodriguez, *Phys. Rev. B* **82**, 014505 (2010).
- ²¹ J.P. Rodriguez, M.A.N. Araujo, P.D. Sacramento, *Phys. Rev. B* **84**, 224504 (2011).
- ²² J.P. Rodriguez, M.A.N. Araujo, P.D. Sacramento, *Eur. Phys. J. B* **87**, 163 (2014).
- ²³ A. Nicholson, W. Ge, X. Zhang, J. Riera, M. Daghofer, A.M. Oles, G.B. Martins, A. Moreo, and E. Dagotto, *Phys. Rev. Lett.* **106**, 217002 (2011); A. Nicholson, W. Ge, J. Riera, M. Daghofer, A. Moreo, and E. Dagotto, *Phys. Rev. B* **85**, 024532 (2012).
- ²⁴ S. Raghu, Xiao-Liang Qi, Chao-Xing Liu, D.J. Scalapino, Shou-Cheng Zhang, *Phys. Rev. B* **77**, 220503(R) (2008).
- ²⁵ J. He, X. Liu, W. Zhang, L. Zhao, D. Liu, S. He, D. Mou, F. Li, C. Tang, Z. Li, L. Wang, Y. Peng, Y. Liu, C. Chen, L. Yu, G. Liu, X. Dong, J. Zhang, C. Chen, Z. Xu, X. Chen, X. Ma, Q. Xue, X. J. Zhou, *Proc. Nat. Acad. Sci.* **111**, 18501 (2014).
- ²⁶ The FeSe monolayer lies on a substrate that may act to preserve tetragonal crystal structure. In the absence of a substrate, which is the case in a bulk crystal of $\text{Ba}_{1-x}\text{K}_x\text{Fe}_2\text{As}_2$, it can be argued that the nematicity in the electronic structure that is observed in the orthorhombic parent compound BaFe_2As_2 pre-empts the predicted Mott transition. See Supplemental Material (I) for Mott transition versus structural transition.
- ²⁷ J.P. Rodriguez, arXiv:1601.07479 .
- ²⁸ Ignoring the contribution of d_{xy} -orbital pairing in the s -wave and in the d -wave channels is a good approximation in the present limit of large on-site Coulomb repulsion. See Supplemental Material (II).
- ²⁹ B.D. Josephson, *Physics Letters* **1**, 251 (1962).
- ³⁰ P.W. Anderson, in *Lectures on the Many-Body Problem*, ed. E.R. Caianiello (Academic, Press, New York, 1964), vol. 2, p. 113.
- ³¹ A.J. Leggett, *Progr. Theor. Phys. (Kyoto)* **36**, 901 (1966).

- ³² A.J. Leggett, *Rev. Mod. Phys.* **47**, 331 (1975).
- ³³ M. Yoshizawa, D. Kimura, T. Chiba, A. Ismayil, Y. Nakanishi, K. Kihou, C.-H. Lee, A. Iyo, H. Eisaki, M. Nakajima, S. Uchida, *J. Phys. Soc. Jpn.* **81**, 024604 (2012).
- ³⁴ M. Yoshizawa and S. Simayi, *Mod. Phys. Lett. B* **26**, 1230011 (2012)
- ³⁵ S. Sachdev, *Quantum Phase Transitions* (Cambridge University Press, Cambridge, 2001).
- ³⁶ Y. Bang, *New J. Phys.* **16**, 023029 (2014).
- ³⁷ F. Kretschmar, B. Muschler, T. Böhm, A. Baum, R. Hackl, Hai-Hu Wen, V. Tsurkan, J. Deisenhofer, and A. Loidl, *Phys. Rev. Lett.* **110**, 187002 (2013).
- ³⁸ T. Bohm, A.F. Kemper, B. Moritz, F. Kretschmar, B. Muschler, H.-M Eiter, R. Hackl, T.P. Devereaux, D.J. Scalapino, and H.-H. Wen, *Phys. Rev. X* **4**, 041046 (2014).
- ³⁹ C.L. Kane, P.A. Lee and N. Read, *Phys. Rev. B* **39**, 6880 (1989).
- ⁴⁰ A. Auerbach and B. E. Larson, *Phys. Rev. B* **43**, 7800 (1991).
- ⁴¹ R.B. Lehoucq, D.C. Sorensen and C. Yang, *ARPACK Users' Guide* (SIAM, Philadelphia, 1998).
- ⁴² K. Seo, B.A. Bernevig and J. Hu, *Phys. Rev. Lett.* **101**, 206404 (2008).
- ⁴³ A.J. Leggett, in *Modern Trends in the Theory of Condensed Matter* (Springer-Verlag, 1980), p. 13; *J. Phys. Col.* **41**, C7-19 (1980).
- ⁴⁴ P. Nozieres and S. Schmitt-Rink, *J. Low Temp.Phys.* **59**, 195 (1985).
- ⁴⁵ H. Yokoyama and M. Ogata, *J. Phys. Soc. Jpn.* **65**, 3615 (1996); A. Paramekanti, M. Randeria and N. Trivedi, *Phys. Rev. B* **70**, 054504 (2004).
- ⁴⁶ Analogs of projected BCS wavefunctions (ref.⁴⁵) for S^{+-} and for D^{+-} pairing symmetries have been written down by the author and S. Haas (unpublished). At half filling and in the vicinity of the QCP, variational Monte Carlo calculations of such pair states on a 6×6 lattice of spin-1 iron atoms yield energy densities $\langle H \rangle / N_{\text{Fe}}$ near the exact groundstate energy density extracted from Fig. 3.
- ⁴⁷ An alternative heuristic form for the condensate of $2N$ holes is given by the “binomial” expression

$$\langle 1, \dots, 2N | \Psi_N \rangle = \frac{1}{\sqrt{2^N (2N)!}} \sum_p (\text{sgn } p) \langle p(1), p(2) | \psi_{J'} \rangle \dots \langle p(2N-1), p(2N) | \psi_{J'} \rangle,$$

where p are permutations.

- ⁴⁸ A.J. Leggett and S. Takagi, *Ann. Phys. (N.Y.)* **106**, 79 (1977).
- ⁴⁹ Ch. Lee, K. Kihou, K. Horigane, S. Tsutsui, T. Fukuda, H. Eisaki, A. Iyo, H. Yamaguchi, A.

- Baron, M. Braden and K. Yamada, *J. Phys. Soc. Jpn.* **79**, 014714 (2010).
- ⁵⁰ M. Rotter, M. Tegel, and D. Johrendt, *Phys. Rev. Lett.* **101**, 107006 (2008).
- ⁵¹ Z.-S. Wang, H.-Q. Luo, C. Ren, and H.-H. Wen, *Phys. Rev. B* **78**, 140501(R) (2008).
- ⁵² D. Sun, Y. Lin, and C.T. Lin, *Phys. Rev.* **80**, 144515 (2009).
- ⁵³ M. Pissas, M. Zeibekis, D. Stamopoulos, C. Wang, and Y. Ma, *Physica C* **476**, 68 (2012).
- ⁵⁴ M.M. Korshunov and I. Eremin, *Phys. Rev. B* **78**, 140509(R) (2008).
- ⁵⁵ T.A. Maier and D.J. Scalapino, *Phys. Rev. B* **78** 020514(R) (2008).
- ⁵⁶ M. Khodas and A.V. Chubukov, *Phys. Rev. Lett.* **108**, 247003 (2012).
- ⁵⁷ D.J. Scalapino and T.P. Devereaux, *Phys. Rev. B* **80**, 140512(R) (2009).

Supplemental Material: Collective Mode at Lifshitz Transition in Iron-Pnictide Superconductors

Jose P. Rodriguez

*Department of Physics and Astronomy,
California State University at Los Angeles, Los Angeles, California 90032.*

I. Mott Transition versus Structural Transition

The two-orbital t - J model [Eq. (1) in the paper] predicts a Mott insulator groundstate at half-filling. Parent compounds to iron-pnictide superconductors at half-filling are bad metals^{S1}, on the other hand, with orthorhombic crystal structure at low temperature^{S2}. Let us simulate the last fact by imposing an orthorhombic shear strain

$$\epsilon_{x'y'} = \frac{1}{2} \left(\frac{\partial u_x}{\partial x} - \frac{\partial u_y}{\partial y} \right) = \frac{a - b}{a + b}, \quad (\text{S1})$$

with new lattice constants $a > b$ such that $a_0^2 = ab$. Here a_0 is the original tetragonal lattice constant. Assume now that the shear strain couples to the emergent electron bands so that the d_{yz} band at $(\pi/a_0)\hat{\mathbf{x}}$ and the d_{xz} band at $(\pi/a_0)\hat{\mathbf{y}}$ respectively shift rigidly up in energy and shift rigidly down in energy by an equal amount proportional to $\epsilon_{x'y'}$. (Cf. ref.^{S3}.) Such a nematic asymmetry between the electronic orbitals may be intrinsically due to the orthorhombic strain, or vice versa^{S2}. In particular, the orthorhombic crystal structure may induce anisotropy in the Heisenberg exchange coupling constants so that commensurate spin-density wave (cSDW) order is established preferentially along the a axis^{S4}, or nematic symmetry breaking could occur because of antiferromagnetic frustration^{S5}. Figure S1a depicts the resulting emergent Fermi surfaces^{S6} of the two-orbital t - J model at the QCP, in the Mott insulator state at half filling. For the sake of clarity, we have turned off hybridization between hole bands with d_{xz} and d_{yz} orbital character. (Cf. Fig. S2.) The Fermi surfaces are no longer nested by $(\pi/a)\hat{\mathbf{x}}$ or by $(\pi/b)\hat{\mathbf{y}}$. Notice also that the system is now orbitally ordered^{S8}, with more electrons populating the d_{xz} versus the d_{yz} orbital.

Emergent nesting along the a axis can be restored if electrons from other orbitals, such as the d_{xy} one, migrate into the d_{xz}/d_{yz} hole bands. Figure S1b depicts the new nesting of

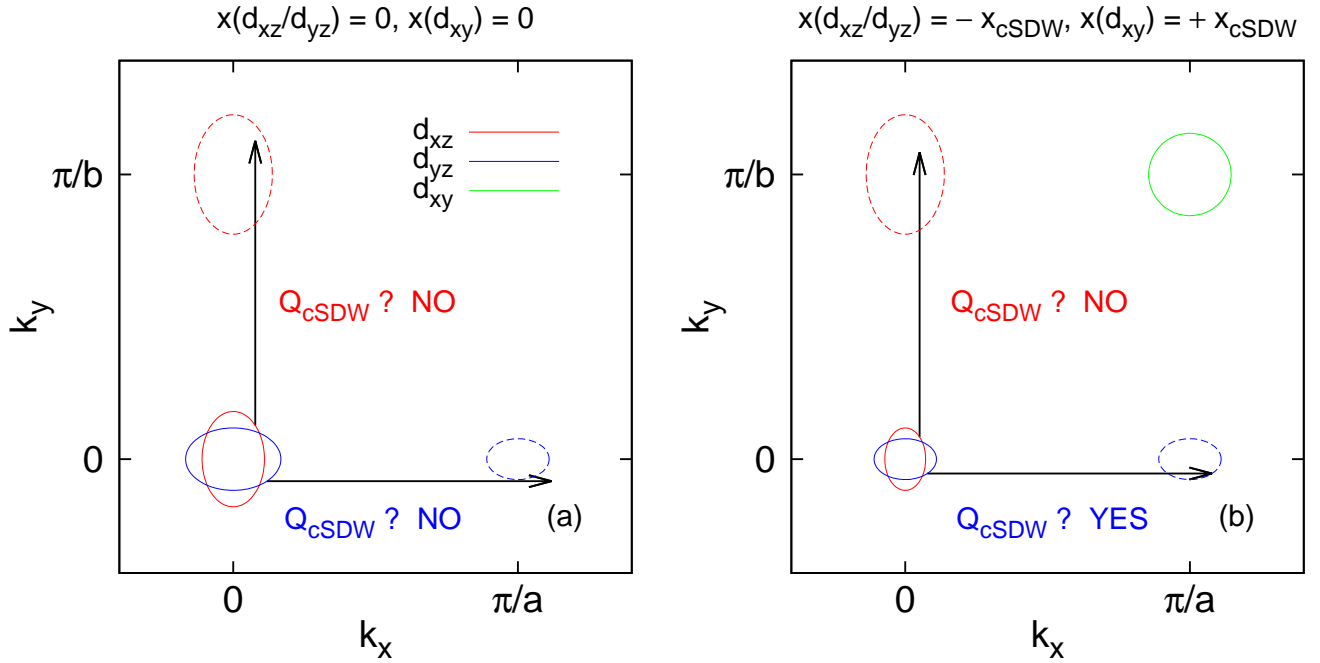


FIG. S1: Fermi surfaces of the two-orbital t - J model (a) at and (b) near half filling. The emergent electron bands in the d_{yz} and in the d_{xz} orbitals are shifted up and down in energy because of an applied orthorhombic shear strain, $(a - b)/(a + b) > 0$. (Cf. ref.^{S3}.) The labels k_x and k_y denote components of pseudo momentum. (See ref.^{S7}).

the Fermi surfaces in such case. It bears some resemblance to the nematicity in the electronic structure of orthorhombic/ c SDW parent compounds to iron-pnictide superconductors revealed experimentally by angle-resolved photoemission spectroscopy (ARPES)^{S9}. Notice the appearance of a new d_{xy} hole pocket that compensates for the reduced area of the d_{xz}/d_{yz} hole pockets in Fig. S1b. Density-functional theory (DFT) calculations predict that such a d_{xy} hole pocket appears upon hole doping from half filling in the absence of electronic nematicity^{S10}. The presence of the d_{xy} hole pocket at half-filling shown in Fig. S1b could be driven by the gain in magnetic energy that results from establishing c SDW order along the a axis. In such case, however, the system is no longer a Mott insulator. Instead, it is a bad metal at half filling, with a low concentration of electrons in the d_{xz}/d_{yz} orbitals overall,

$x_{cSDW} \propto \epsilon_{x'y'}$, compensated by an equal concentration of holes in the d_{xy} orbital.

II. Electron d_{xy} Pairing at Strong On-site Coulomb Repulsion

The limit of strong on-site Coulomb repulsion, which is adopted in the paper, puts severe restrictions on the pairing symmetry in iron-pnictide superconductors. Let us define the pairing function of the superconducting groundstate in the usual way: $iF_{i,\alpha;j,\beta} = \langle c_{i,\alpha,\uparrow}^\dagger c_{j,\beta,\downarrow}^\dagger \rangle$, where i and j denote iron sites, and where α and β are d_{xz} , d_{yz} or d_{xy} orbitals. The limit $U_0, U'_0 \rightarrow \infty$ then imposes the constraints $iF_{i,\alpha;i,\beta} = 0$ at all sites i . Application of translational invariance yields one constraint,

$$\sum_{\mathbf{k}} \langle c_{\alpha,\uparrow}(\mathbf{k})^\dagger c_{\beta,\downarrow}(-\mathbf{k})^\dagger \rangle = 0. \quad (\text{S2})$$

The sum in momentum above is over the one-iron (unfolded) Brillouin zone, while $c_{\alpha,s}(\mathbf{k}) = N_{\text{Fe}}^{-1/2} \sum_i e^{-i\mathbf{k}\cdot\mathbf{r}_i} c_{i,\alpha,s}$ destroys a spin- s electron in orbital α that carries momentum $\hbar\mathbf{k}$. The latter coincides with the crystal momentum if the two iron sites per iron-pnictide unit cell are equivalent. It represents the pseudo momentum connected with the glide-reflection symmetry shown by an isolated iron-pnictide layer if the two iron atoms per unit cell are inequivalent^{S7}. The pseudo momentum coincides with the one-iron crystal momentum in the case of an electron in a d_{xz}/d_{yz} orbital, while these two momenta differ by a reciprocal lattice vector $(\pi/a)(\hat{x} \pm \hat{y})$ in the case of an electron in the d_{xy} orbital. Figure S2 depicts a typical Fermi surface for iron-pnictide materials in the one-iron Brillouin zone and in the two-iron Brillouin zone as predicted by density-functional theory^{S10}. Below, we list the restrictions on d_{xy} pairing when constraint (S2) is enforced.

S-wave Cooper Pair. Suppose that $\alpha = d_{xy} = \beta$ in the constraint (S2). Then study of the Fermi surfaces depicted in Figs. S2a and S2b imply that isotropic pairing is ruled out. Next, suppose instead that $\alpha = d_{xy}$ and that $\beta = d_{yz}$. Again, the constraint (S2) is incompatible with Figs. S2a and S2b, which means that s -wave pairing is ruled out once more.

D-wave Cooper Pair. Consider again the diagonal orbital channel $\alpha = d_{xy} = \beta$. Figure S2 shows that $D_{x^2-y^2}$ pairing is possible in this channel, which satisfies the constraint (S2). In the particular case of inequivalent iron atoms, Fig. S2b indicates that d_{xz}/d_{yz} pairing is nodeless, while that d_{xy} pairing has nodes. This implies that the former is the dominant pairing channel in such case. In the off-diagonal orbital channel, $\alpha = d_{xy}$ and $\beta = d_{yz}$, Fig.

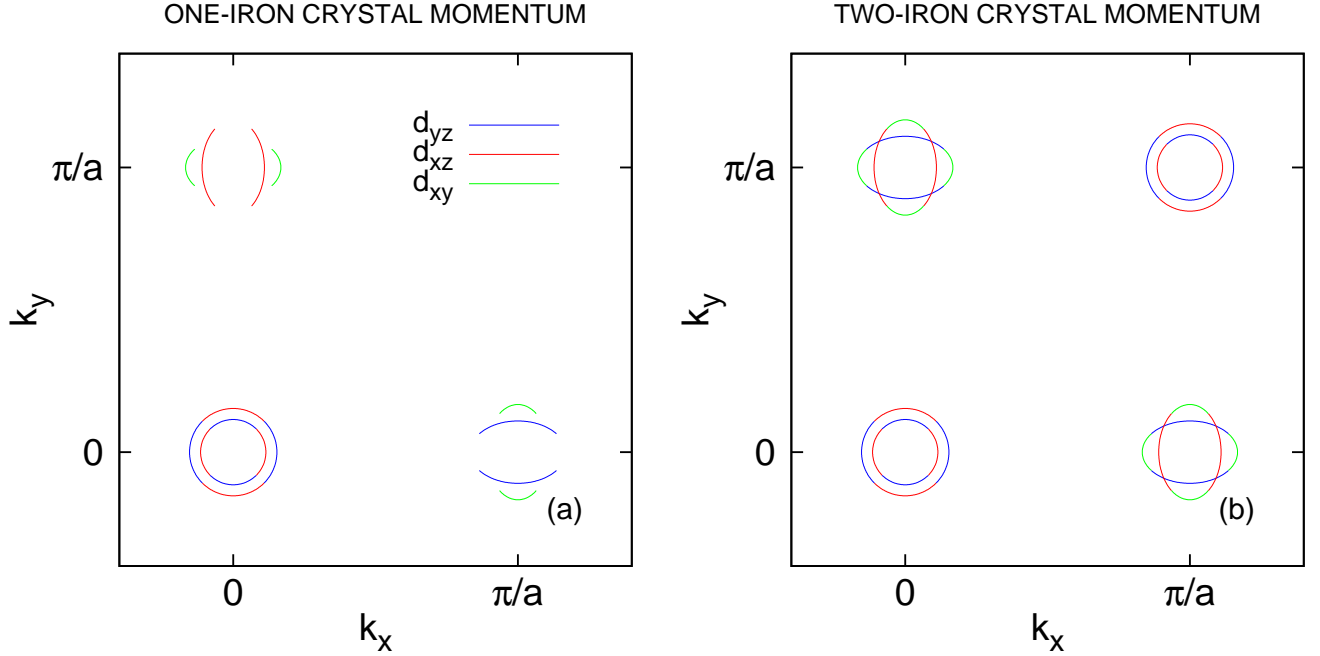


FIG. S2: Sketch of the typical Fermi surfaces predicted by DFT for iron-pnictide materials near half filling. (See ref.^{S10}.) Panels (a) and (b) correspond, respectively, to equivalent and to inequivalent iron atoms per iron-pnictide unit cell.

S2a in conjunction with (S2) imply that $D_{x^2-y^2}$ pairing is ruled out in the case of equivalent iron atoms. The same holds true in the case of inequivalent iron sites, Fig. S2b. In the latter case, specifically, D_{xy} pairing is possible in this off-diagonal orbital channel, but it has nodes. It will therefore be smaller in amplitude than the dominant d_{xz}/d_{yz} orbital channel for $D_{x^2-y^2}$ pairing discussed previously.

P-wave Cooper Pair. Study of Fig. S2 yields that P_x triplet pairing is generally possible in the diagonal orbital channel $\alpha = d_{xy} = \beta$, which again satisfies the constraint (S2). Both this pair wave function and the d_{yz} counterpart show nodes. This indicates that they are competing pair states with comparable magnitudes. Next, set $\alpha = d_{xy}$ and $\beta = d_{xz}$ in the constraint (S2). Inspection of Fig. S2 yields that P_x triplet pairing is possible in this off-diagonal orbital channel as well, but only in the case of inequivalent iron sites. In principle,

it is comparable in magnitude to d_{yz} - d_{yz} triplet P_x pairing, but it lives in a much reduced momentum space in between the principal axes.

-
- [S1] M. Nakajima, S. Ishida, T. Tanaka, K. Kihou, Y. Tomioka, T. Saito, C.-H. Lee, H. Fukazawa, Y. Kohori, T. Kakeshita, A. Iyo, T. Ito, H. Eisaki, and S. Uchida, *J. Phys. Soc. Jpn.* **83**, 104703 (2014).
- [S2] S. Nandi, M. G. Kim, A. Kreyssig, R. M. Fernandes, D. K. Pratt, A. Thaler, N. Ni, S. L. Bud'ko, P. C. Canfield, J. Schmalian, R. J. McQueeney, and A. I. Goldman, *Phys. Rev. Lett.* **104**, 057006 (2010).
- [S3] M. Yoshizawa and S. Simayi, *Mod. Phys. Lett. B* **26**, 1230011 (2012)
- [S4] B. Schmidt, M. Siahatgar, and P. Thalmeier, *Phys. Rev. B* **81**, 165101 (2010).
- [S5] C. Xu, M. Muller, and S. Sachdev, *Phys. Rev. B* **78**, 020501(R), (2008).
- [S6] J.P. Rodriguez, M.A.N. Araujo, P.D. Sacramento, *Eur. Phys. J. B* **87**, 163 (2014).
- [S7] P.A. Lee and X.-G. Wen, *Phys. Rev. B* **78**, 144517 (2008).
- [S8] Y. Yanagi, Y. Yamakawa, N. Adachi, and Y. Ono, *Phys. Soc. Japan* **79**, 123707 (2010).
- [S9] M. Yi, D. Lu, J.G. Analytis, A.P. Sorini, A.F. Kemper, B. Moritz, S.-K. Mo, R.G. Moore, M. Hashimoto, W.-S. Lee, Z. Hussain, T.P. Devereaux, I.R. Fisher, and Z.-X. Shen, *Proc. Nat. Acad. Sci.* **108**, 6878 (2011).
- [S10] A.F. Kemper, T.A. Maier, S. Graser, H.-P. Cheng, P.J. Hirschfeld, and D.J. Scalapino, *New J. Phys.* **12**, 073030 (2010).